Optics and Lasers in Engineering 135 (2020) 106193

Contents lists available at ScienceDirect

Optics and Lasers in Engineering

journal homepage: www.elsevier.com/locate/optlaseng

Review

# Status, challenges, and future perspectives of fringe projection profilometry

Jing Xu[a], Song Zhang[b,*]

[a] Department of Mechanical Engineering, Tsinghua University, Beijing, China 100084
[b] School of Mechanical Engineering, Purdue University, West Lafayette, Indiana 47907, USA

ARTICLE INFO

*Keywords:*
Fringe projection
3D Sensing
3D Imaging
Structured light
Perception
Robotics

ABSTRACT

As one of the most popular techniques for non-contact three-dimensional (3D) sensing/imaging, fringe projection profilometry (FPP) has been growing rapidly over the past decades partially because of the improved speed of computing devices and reduced cost of hardware. 3D optical sensing has started being an integral part of our daily lives such as Face ID enabled by 3D sensors on smart phones. The impact of such techniques can be even greater with the ever-growing artificial intelligent (AI), machine learning, smart manufacturing, robotics as well as other fields. However, there are still fundamental challenges to be tackled to make such advanced optical sensing techniques ubiquitous. This paper presents the current status of FPP techniques, the major challenges still facing in the field, and our perspectives on the future of FPP techniques.

## 1. Introduction

3D optical imaging/sensing, a technology that acquires surface geometry information without physically touching it, has seen its integration and application to fields ranging from entertainment, manufacturing, to healthcare industry. Yet, its potential has far from been reached, partially due to the low technological mature level and the lack of intelligence.

Let us take a look at a scenario when 3D optical imaging technology could play a critical role but the technology is not yet ready. Human has successfully sent robots to the Mars for space exploration (an unknown and unstructured environment). Ideally, the robots can have human like body, human like hands, and human like eyes that can take actions like human when human cannot physically go there because the environment is too dangerous or not friendly to human. Through sensing and perception, robots can gather all necessary information for human to understand the Mars; and if robots are smart enough, they can explore the Mars as human would do. However, these seemingly achievable goals are still far away. This scenario actually has three major components: perception/sensing systems that should be able to accurately and robustly capture an unknown scene; the intelligent system to precisely understand the captured data and extrapolate the useful information; and the control system that can take actions (e.g., grasping). The former two are directly related to the major topic covered in this paper: 3D optical imaging/sensing, and the last one could be related, as well, if the control system requires the sensed data for closed-loop control. As such, this paper will present the state-of-the-art 3D optical imaging techniques, the technological gaps, and the remaining challenges for us to accomplish such a mission.

3D optical imaging techniques can be classified into two major categories, the passive methods and the active methods. A passive method reconstructs 3D scenes from naturally illuminated images acquired from a single view with different conditions (e.g., defocusing level) or multiple views [1,2]. Among all existing 3D optical imaging techniques, the stereo-vision technique is probably the most extensively employed and well studied one. Stereo-vision technique generates 3D point through triangulating the corresponding pairs between stereo images. Since only two cameras are used, the stereo-vision technique has obvious advantages: the simplicity of hardware configuration and straightforward calibration for the system [3]. However, stereo-vision technique measurement accuracy is determined by the accuracy of determining corresponding pairs, resulting in low measurement accuracy for object without rich texture. In fact, this approach completely fails if the object does not present texture on camera images. As such, the fundamental stereo-vision problem is often considered as a "ill-posed" problem.

Active methods overcome the fundamental problem related to natural texture by actively illuminating object with "known" signal such that the detector can uniquely identify from the captured signal. The signal can be modulated light in time domain such that the distance can be measured by finding the travel time of the signal (e.g., time of flight or TOF [4]). Due to its small footprint and possible compact design, TOF technique is quite extensively used in long range measurement, and recently for short-range measurement as well. However, the achievable depth resolution for short-range measurement is still low comparing with triangulation based approach primarily because the limited resolution of the detector to gauge time delay.

* Corresponding author.
*E-mail address:* szhang15@purdue.edu (S. Zhang).

https://doi.org/10.1016/j.optlaseng.2020.106193
Received 28 September 2019; Accepted 11 May 2020
Available online 4 June 2020

The actively signal can be modulated in spatial domain such that the correspondence between illuminator and the camera image can be established. The technique of projecting spatially modulated signal for 3D imaging is often regarded as *structured light* technique. Structured light technique gains its popularity because consumer electronics (e.g., iPhone X) adopt such a technique. In the iPhone X case, the illuminator is a random dot projector that generates a unique dot distribution locally, from which the camera can find the corresponding point within a window using a digital image correlation (DIC) technique. Alternatively, the locally unique illumination distribution can be created by natural laser speckle [5] or a digital video projector [6]. The advantage of this approach is a single pattern is sufficient for 3D imaging, achieving highest possible measurement speed (i.e., as fast as the camera). However, because the dot distribution is discrete in 2D, the measurement resolution is limited in both directions [7]. Furthermore, the correspondence accuracy is affected by the illumination distribution, and thus the depth resolution is also limited.

The active signal can also be both spatially and temporally modulated. Overall, the method using both spatially and temporally modulated signal could achieve higher resolution than the method using spatially or temporally modulated signals. The spatially and temporally modulated patterns are often realized by a digital video projector because of its flexibility and versatility, albeit they can also be realized by laser speckles [8], or mechanically moving object [9,10], or LED arrays [11,12]. The codification methods, strategies and limitations have been well discussed by Salvi et al. [6] and Zhang [7], and the state-of-the-art 3D imaging techniques have been reviewed by various authors in differential categories [7,13–19].

This paper will not exhaustively cover all 3D optical imaging technologies. Instead, this paper primarily focuses on one spatial type of structured light techniques called *fringe projection profilometry* or FPP because of its achievable speed, resolution, accuracy, affordability, and versatility. As such, this advanced 3D imaging technology might greatly impact numerous more fields than it has right now. Moreover, we will present a few application examples (e.g., cardiac mechanics, robotics, additive manufacturing, forensic science, entertainment) to better convey the challenges and future perspectives.

## 2. Current status

This section introduces the basic principle of structured light technique; and summarizes various aspects of the current status of fringe projection profilometry, namely, fringe pattern generation, fringe pattern analysis, absolute phase retrieval, system calibration, 3D reconstruction, as well as high speed realization and high dynamic range (HDR) methods.

### 2.1. Basic principle

Structured light techniques originated from the conventional stereo vision method that recovers 3D information by imitating human perception system. As mentioned above, structured light technique eliminates the fundamental correspondence problem of a stereo-vision technique by replacing one of the cameras with a projector and actively projecting known feature points [6]. Fig. 1 schematically illustrates the basic configuration of a 3D imaging system using a structured light method. The system comprises of a projection unit that shines structured patterns onto the object surface, and an image acquisition unit that captures the structured pattern scattered by object surface from a different perspective. The surface geometry distorts the projected patterns and the software algorithm analyzes pattern distortions for 3D shape recovery. Because the projected patterns have known features, the correspondence can be more easily established even on the distorted image captured by the camera. A system calibration technique, to be discussed later, typically provides the triangulation relationship between the projection unit and the acquisition unit, and then a corresponding pair can be used

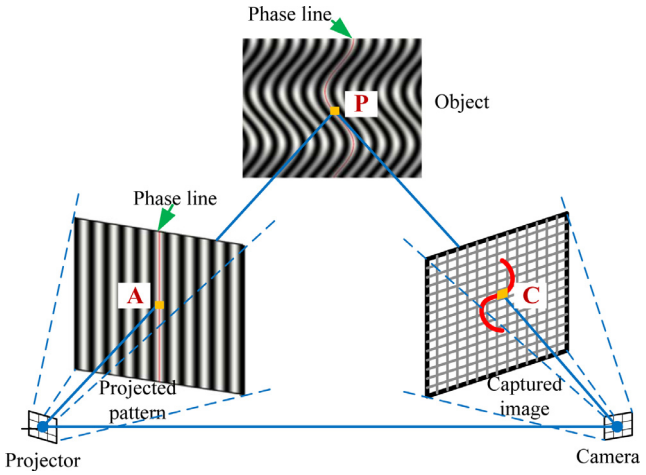


**Fig. 1.** Schematic diagram of a typical structured light system [7].

to reconstruct 3D coordinates, $(x^w, y^w, z^w)$, based on the triangulation relationship, which will be detailed in Section 2.5.

Ultimately, by projecting pre-defined structured pattern(s), the structured light technique can uniquely and robustly determine a corresponding projector point $(u^p, v^p)$ for a given camera point $(u^c, v^c)$ on the camera image. Historically, numerous structured pattern encoding methods have been developed including the statistically random pattern (dots or speckle), binary coded patterns, multi-level patterns, triangular patterns, trapezoidal patterns, pyramid patterns, sinusoidal patterns. The statistically random pattern ensures that a kernel of $w_m \times w_n$ pixels is unique within region of interest. Due to its simplicity, low cost, and easy to be miniaturized, this method saw its great success in developing low-cost consumer-level 3D sensors ((e.g., Microsoft Kinect V1, Intel RealSense R200, iPhone X, Orbbec Astro series). However, such a method has a relatively low spatial resolution in both $u$ and $v$ direction because the random pattern is discrete in both directions. And because its low spatial resolution leads to low correspondence determination accuracy, the achievable depth accuracy is typically not high.

Due to the inherent existence of geometric constraint of the structured light system, the unique correspondence is required only in one dimensional (1D) by leveraging the *epipolar geometry* developed in a traditional stereo-vision system [20,21] to uniquely determine the corresponding point in the second dimension. As such, the encoded structured patterns only need to vary in 1D, but remain constant and continuous in the second dimension. Binary coding methods were then developed. For such methods, each stripe on the projector is encoded with a unique code (i.e. codeword) that can be realized by projecting a sequence of binary patterns. Assume black represents 0 and white represents 1, the sequence of patterns captured by the camera can be used to determine the codeword for each point that uniquely gives the corresponding stripe on the projector. The binary coding method boots the spatial resolution by achieving camera pixel level resolution in the direction that the structured patterns remain constant. However, this technique requires the projection of many binary patterns, making it difficult to achieve high measurement speed without utilizing specialized hardware, albeit there were some successes by developing a specialized coding strategy [22,23], utilizing color [24] or multi-level grayscale structured patterns [25], as well as adding a second camera [26–28]. Furthermore, its spatial resolution cannot reach camera pixel level in the direction that the patterns vary.

### 2.2. Fringe pattern generation

FPP is a method that reconstruct 3D information by analyze fringe pattern(s). *Fringe* is conventionally defined as a structured pattern that varies sinusoidally. In this paper, we generalize this pattern definition

by removing the sinusoidal constraint because the new analysis method can process non-sinusoidal pattern(s) in a similar manner for 3D shape reconstruction. As such, more fringe generation methods can be used for FPP. The following methods have been successfully developed and extensively employed for 3D shape reconstruction.

- *Interference.* Based on the property of electromagnetic wave of a coherent laser source, superposing two laser beams with the same wavelength together naturally generates a sinusoidal pattern. And the method that using this type of fringe pattern generation is called interferometry [29].
- *Physical grating projection.* Before digital video projection devices become popular and affordable, sinusoidal fringe patterns can be made as a grating [30], or printed on a transparency film [31]. The physically made pattern is then projected by projection optics.
- *Moiré.* Moiré fringes are large-scale interference patterns that can be produced when an opaque ruled pattern with transparent gaps is overlaid on another similar pattern [32].
- *Digital video projection.* Digital video projectors make it easier to produce fringe patterns generated by a computer [13]. Since such fringe patterns can be digitally created, digital fringe projection techniques have a lot more flexibilities than those physical grating methods.

Lately, researchers have demonstrated that binary patterns could also be used to achieve equally high-quality 3D imaging and further break speed grounds. These new developments include generating fringe patterns with the out-of-focused squared binary patterns [33], the pulse width modulated patterns [34–36], the binary dithered patterns [37], the optimized dithered patterns [38–44], and the mechanically spinning grated patterns [9,10]. Due to the flexibility of the digital pattern projectors, researchers also developed techniques that uses more than 2 gray-scale values [45], or combination of multiple binary patterns for a single fringe pattern [46–49].

### 2.3. Fringe analysis

Instead of using image intensity, fringe projection techniques use the phase for 3D reconstruction. Over the years, numerous fringe analysis methods have been developed, and here we only summarize those most popular ones.

An ideal sinusoidal fringe image can be mathematically described as

$$I_1(x,y) = I'(x,y) + I''(x,y)\cos[\phi(x,y)], \tag{1}$$

where $I'(x, y)$ is the average intensity or the DC component, $I''(x, y)$ the intensity modulation, and $\phi(x, y)$ the phase to be solved for.

Theoretically, the single fringe pattern is sufficient to obtain the phase value, and such a method is called Fourier transform profilometry (FTP), developed by Takeda and Mutoh in 1983 [50]. FTP method works as follows, re-write Eq. (1) in a complex form as

$$I_1(x,y) = I'(x,y) + 0.5\cdot I''(x,y)\left[e^{j\phi(x,y)} + e^{-j\phi(x,y)}\right], \tag{2}$$

where $e^{j\phi(x,y)}$ is the conjugate of $e^{-j\phi(x,y)}$.

Then apply a band-pass filter in frequency domain to remove the conjugate and DC component such that,

$$\tilde{I}_1(x,y) = 0.5\cdot I''(x,y)e^{j\phi(x,y)}. \tag{3}$$

Finally find the phase $\phi(x, y)$ by

$$\phi(x,y) = \tan^{-1}\left\{\frac{\Im[\tilde{I}(x,y)]}{\Re[\tilde{I}(x,y)]}\right\}. \tag{4}$$

Here $\Im()$ and $\Re()$ respectively denotes the imagery and real part of a complex variable. Since an arctangent function is used here, Eq. (4) only produces a phase map ranging from $[-\pi, +\pi)$ with a $2\pi$ modus, and the recovered phase map is thus called *wrapped phase*. If a continuous phase map is required, a step called phase unwrapping is necessary. Various phase unwrapping methods and the current status will be discussed in Section 2.4.

Furthermore, $I''(x, y)$ can also be recovered by applying a low-pass filter to Eq. (1), and the resultant image is often used as a texture or photograph of the object for better visualization or analysis.

The aforementioned simple FTP method works well if surface geometry is smooth, fringe noise level is not too high, and surface texture is not rich. However, most practical applications are rather complex and the simple FTP method does not work well. One of the most challenging problems associated with single fringe phase analysis method is to cleanly separate carrier phase signal from the background (e.g., DC). New analysis methods have been developed to alleviate problems associated with the simple FTP method, such as windowed Fourier transform [51–54], multiscale windowed Fourier transform [55], Wavelet transform [56–60], Hilbert transform [61,62], DC signal elimination [63,64], or machine learning methods [65,66]. Despite these advancements, the single fringe based phase recovery method is still limited to measure certain type of objects. Therefore, capturing more fringe patterns can theoretically enhance the measurement quality and improve the measurement capacity.

To completely eliminate background impact, Mao et al. [67] proposed to capture the second $\pi$-shifted pattern, i.e.,

$$I_b(x,y) = I'(x,y) + I''(x,y)\cos[\phi(x,y)+\pi], \tag{5}$$

by taking the difference between these two patterns

$$I_d(x,y) = I_1(x,y) - I_b(x,y) = 2I''(x,y)\cos[\phi(x,y)], \tag{6}$$

the DC component is completely eliminated, assuming that the measurement conditions remain the same. This method is called the modified Fourier transform method. Alternatively, Guo and Huang [68] proposed to directly capture the DC image, i.e., $I_b(x, y) = I'(x, y)$. The difference between these two approach is that the former has better signal to noise ratio but the latter is less sensitive to motion introduced error. Since the DC component does not present, these two fringe based methods can substantially improve measurement quality and also tolerate surface texture to a certain degree. Fringe analysis methods with a single or dual fringe patterns have been extensively employed for high-speed applications [16,17,69,70]. However, they typically requires surface to be at least locally smooth and have no strong texture variations, and thus fringe analysis with more fringe patterns are necessary to relax strong requirements.

Since Eq. (1) has three unknowns $I'(x, y)$, $I''(x, y)$, and $\phi(x, y)$, three equations are sufficient to determine the phase $\phi(x, y)$ pixel by pixel. One of the most straightforward approach is to add one sinusoidal fringe pattern and another DC image [71],

$$I_2(x,y) = I'(x,y) + I''(x,y)\sin[\phi(x,y)], \tag{7}$$

$$I_3(x,y) = I'(x,y). \tag{8}$$

In this case, the phase can be calculated as

$$\phi(x,y) = \tan^{-1}\left[\frac{I_2(x,y) - I_3(x,y)}{I_1(x,y) - I_3(x,y)}\right]. \tag{9}$$

Three or more phase-shifted fringe patterns with known phase shifts are also developed to recover phase pixel by pixel, and those methods are called phase-shifting methods [72]. Phase-shifting methods have been extensively employed in optical metrology due to its speed, accuracy, resolution, and robustness. Assume the $i-th$ image with a phase shift of $\delta_i$ is written as,

$$I_i(x,y) = I'(x,y) + I''(x,y)\cos[\phi(x,y)+\delta_i], \tag{10}$$

the phase can be solved by

$$\phi(x,y) = \tan^{-1}\left[\frac{-a_2(x,y)}{a_1(x,y)}\right], \tag{11}$$

where

$$\begin{bmatrix} a_0(x,y) \\ a_1(x,y) \\ a_2(x,y) \end{bmatrix} = \mathbf{A}^{-1}(\delta_i)\mathbf{B}(x,y,\delta_i), \tag{12}$$

here

$$\mathbf{A}(\delta_i) = \begin{bmatrix} N & \sum \cos(\delta_i) & \sum \sin(\delta_i) \\ \sum \cos(\delta_i) & \sum \cos^2(\delta_i) & \sum \cos(\delta_i)\sin(\delta_i) \\ \sum \sin(\delta_i) & \sum \cos(\delta_i)\sin(\delta_i) & \sum \sin^2(\delta_i) \end{bmatrix}, \tag{13}$$

and

$$\mathbf{B}(x, y, \delta_i) = \begin{bmatrix} \sum I_i \\ \sum I_i \cos(\delta_i) \\ \sum I_i \sin(\delta_i) \end{bmatrix}. \tag{14}$$

Various phase-shifting algorithms are thoroughly compared by Zuo et al[19]., and those algorithms applicable for high-speed applications are summarized by Zhang [7]. We encourage readers refer those previous papers for detailed insights and comparing results.

### 2.4. Phase unwrapping

The phase obtained from fringe analysis technique is required to be unwrapped before 3D coordinates conversion. Phase unwrapping essentially determines the integer number $k(x, y)$ of $2\pi$'s to be added to each point to remove those $2\pi$ discontinuities. The state-of-the-art phase unwrapping algorithms can be classified into the following major categories: spatial phase unwrapping, temporal phase unwrapping, geometric-constraint-based phase unwrapping, pre-knowledge-based phase unwrapping, and the hybrid phase unwrapping methods [73].

A *spatial phase unwrapping method* unwraps the phase by referring phase values of other points on the same phase map assuming the surface geometry is smooth. A variety of phase unwrapping methods and algorithms were summarized in the book edited by Ghiglia and Pritt [74]. If a phase map is noise free and object surface is smooth, spatial phase unwrapping methods can work well. Due to the existence of noise, robustly unwrapping the entire phase map remains a challenging problem in general. Among all spatial phase unwrapping algorithms developed, the quality-guided phase unwrapping methods tend to achieve the combined robustness and efficiency. Basically, the quality-guided phase unwrapping method unwraps higher quality phase points before lower quality phase object to reduce the probabilities of incorrectly unwrapped phase points. The review paper written by Su and Chen [75] covered a wide range of quality-guided phase unwrapping algorithms, and the review paper written by Zhao et al. [76] compared different strategies of generating a quality map for robust phase unwrapping. Although numerous algorithms have been developed over the past decades, the spatial phase unwrapping algorithm has some fundamental limitations: 1) assume the surface to be *smooth* at least along one unwrapping path such that the object surface geometry will not introduce more than $\pi$ phase changes between two successive points along the path; and 2) can nly provide *relative* unwrapped phase map (i.e. the absolute position between isolated smooth patches cannot be recovered). It should be noted that attempts have been made to identify the absolute phase position of a single or multiple smooth patches typically be encoding fringe patterns with certain markers [77–84]. These marker encoded methods assume that 1) the surface can be segmented into smooth regions, and for each region, a spatial phase unwrapping can successfully unwrap the entire phase; and 2) the encoded marker is clearly visible and accurately determined for each labelled region [73].

In contrast, a *temporal phase unwrapping* algorithm unwraps the phase for each pixel by referring the temporarily acquired information on the same pixel without referring the neighboring information. As a result, the smoothness requirement for the spatial phase unwrapping is no longer necessary, and the position between isolated smooth patches can also be properly recovered. Conventional temporal phase unwrapping methods, originated from laser interferometry including two- to multi-wavelength phase shifting algorithms [85–87], were successfully employed in laser interferometry systems. These methods essentially generates an equivalent phase map $\Phi^e(x, y)$ by combining the wrapped phase maps of two or more frequencies such that the equivalent phase map does not have $2\pi$ discontinuities. The equivalent phase map is then used to subsequently unwrap the wrapped phase map pixel by pixel. For each algorithm, the robustness to noise varies with the choice of frequencies and the number of frequency employed [88], as well as the employed post-processing algorithm [89].

The temporal phase unwrapping algorithm developed for laser interferometry systems can be directly brought into FPP systems. However, FPP systems have a lot more options for temporal phase unwrapping due to the flexibility of pattern generation.These temporal phase unwrapping algorithms include directly capturing a sequence of fringe patterns carrying equivalent phase $\Phi^e(x, y)$ [90–92], a sequence of binary coded patterns [93–97], a single or multiple gray-coded patterns [98,99], a single statistic pattern [100], several composite fringe patterns with each fringe pattern including multiple frequency components [92,101,102], a stair pattern [103], or several fringe patterns with stair phase encoded [104–109]. The large temporal phase unwrapping portfolio for FPP techniques allows users more flexility to chose a proper algorithm for a given application.

Due to reduced costs of hardware devices, more hardware components (e.g., projector or camera) are integrated into the single 3D imaging system, and the inherent geometric constraints were leveraged for phase unwrapping as well, and such an unwrapping method is regarded as the *geometric-constraint-based phase unwrapping*. By adding one or more hardware components to a single projector and a single camera system, the multiview system provides opportunities to determine the number of $2\pi$'s for phase unwrapping by referring to geometric constraints imposed by additional view(s) [110–117] without temporally capturing additional patterns. Since no additional images are required, these phase unwrapping methods are suitable for high-speed applications. However, the processing speed is rather slow because it typically requires the backward and forward checking. An et al. [118] developed the geometric-constraint based phase unwrapping method that generates a *virtual* reference phase map to unwrap the phase pixel by pixel for the single camera and singe projector system. Later, researchers extended the geometric constraints based phase unwrapping methods by directly capturing the reference plane [119,120], by employing different strategies to determine the virtual reference phase [121,122], or by producing different fringe patterns [123].

Nowadays, most fabricated parts have computer-aided-design (CAD) models, and thus the CAD models can be used as reference for phase unwrapping [124]; and some may have rough 3D measurements acquired by a low-quality device or elsewhere, the lower-quality 3D geometry can also be used for phase unwrapping [125]. The method using the prior ideal or rough geometric information for phase unwrapping is regarded as the *pre-knowledge-based phase unwrapping*.

In addition, some *hybrid phase unwrapping* methods were also developed lately as well. For example, researchers have developed phase unwrapping algorithms by combining the geometric-constraint-based phase unwrapping method with temporal phase unwrapping algorithm [109,126,127], using one coded pattern plus geometric-constraint-based phase unwrapping [128], or using stereo-vision cameras to obtain rough 3D geometry that is further used for phase unwrapping [10,116,129].

### 2.5. System calibration

To convert corresponding pair information in camera/projector pixels to actual 3D information, structured light system calibration is required. The calibration process could be simple or complex, and the achievable accuracy level could be different. Over the years, numerous system calibration methods have been developed. These methods can be classified into three categories: the reference-based methods, the geometric calibration based methods, and the hybrid methods. The simplest reference-plane-based approach works as follows: captures the phase map of a flat object in the field of view, $\Phi^r$; measures the phase

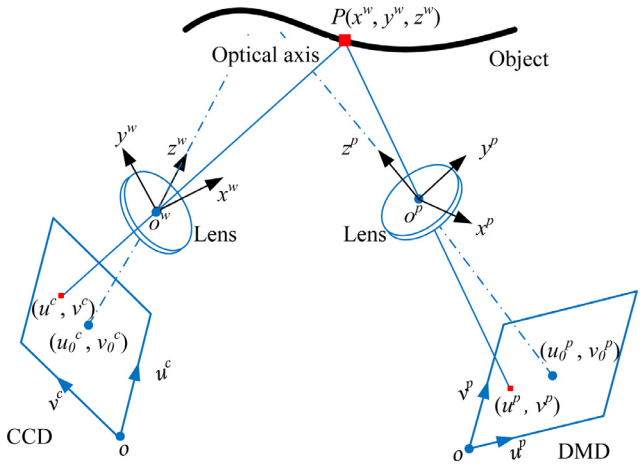


**Fig. 2.** Pinhole model for fringe projection system with the world coordinate system coinciding with the camera lens coordinate system [7].

of the object surface $\Phi^o$; takes the difference of these two phase maps $\Delta\Phi = \Phi^o - \Phi^r$; and calculate depth information as $z \approx c \times \Delta\Phi$, where $c$ is a constant determined by measuring a known height object. $(x, y)$ is obtained by simple scaling the camera pixel coordinates $(u^c, v^c)$. This approximation method can work well for an ideal telecentric system such as those virtually built systems [130], but the approximation error could be large for non-ideal systems [131]. More accurate reference-plane-based methods have been developed [132–147] that better model the relationship between the phase and the depth $z$ through polynomial fitting or piecewise linear fitting. These calibration approaches eachieve various levels of accuracy depending upon the target as well as its movement accuracy.

The geometric calibration approach evolves from those developed in the field of computer vision. This method mathematically represents the camera and the projector as a pinhole model [148], as shown in Fig. 2. And the linear pinhole model can be written as,

$$[u^c, v^c, 1]^T = \mathbf{A} \cdot [\mathbf{R}, \mathbf{t}] \cdot [x^w, y^w, z^w, 1]^T, \tag{15}$$

describing the transformation from the world coordinate system $(x^w, y^w, z^w)$ to the lens coordinate system $(x^c, y^c, z^c)$ and the projection from the lens coordinate system to the image plane $(u^c, v^c)$. Here $^T$ denotes matrix transpose; $\mathbf{A}$ is a $3 \times 3$ intrinsic matrix that models the focal length along $u$ and $v$ direction, and intersection points between optical axis and the imaging plane (i.e., the principle point); $\mathbf{R}$ is a $3 \times 3$ rotation matrix and $\mathbf{t}$ is a $3 \times 1$ translation vector, and matrix $[\mathbf{R}, \mathbf{t}]$ describes the transformation from the world coordinate system to the lens coordinate system. Matrix $[\mathbf{R}, \mathbf{t}]$ is often regarded as the *extrinsic parameters* matrix, and matrix $\mathbf{A}$ is regarded as the *intrinsic parameters* matrix.

It should be noted that the linear lens model works well for high-quality lenses, however, a practical lens might have distortion and thus the nonlinear distortion has to be considered. The primary distortion includes tangential distortion and radial distortion that can be also be mathematically modeled. However, for lens with fabrication artifacts, none of the existing models can work well, and thus the residual error caused by lens artifacts should be compensated for a high accuracy measurement system.

Camera calibration essentially estimates those unknown intrinsic and extrinsic parameters of the imaging system through optimization. The camera calibration has been well studied with some being more complex than others [149–151]. The calibration process was drastically simplified and more flexible with the method developed Zhang [148], and such a method only requires to freely move a flat calibration target with known features on the surface. There are easy-to-use open-source camera calibration software packages (e.g., OpenCV calibration toolbox) for practical use immediately.

The difficulty of fringe projection system calibration lies in the projection unit calibration since a projection unit cannot capture images like the camera. The aforementioned reference-plane based methods basically do not directly calibrate the projector, and the indirect calibration process could lead to lower accuracy or more rigorous requirements on the calibration process. As a result, geometric calibration methods developed for fringe projection system are difficult and complex [152–158]. In 2006, Zhang and Huang [131] developed a simple and flexible method for fringe projection system calibration. By projecting a sequence of fringe patterns onto the object and capturing those patterns with a camera, this method allows the projector "capture" images like a camera. Since the projector can capture images freely, the difficult projector calibration problem becomes a well-established camera calibration problem, and thus the fringe projection system calibration can follow exactly the same process for standard stereo-vision system calibration. Variations of such a calibration approach [159–168] have been developed by different research teams along the direction to improve certain aspects of the calibration process.

Most of the aforementioned system calibration approaches assume that both the projector and the camera are at least nearly focused and they largely follow pinhole models. Researchers have developed calibration approach that allows the projector to be out-of-focus [169], the camera to be out of focus [170], or the use of a spinning fringe projector [171]; and these recent developments could further simplify the calibration process. Researchers have also developed calibration methods that could use single and dual telecentric lenses [172–177], allow using inaccurate calibration target [178], or enable self-calibration [179]. Furthermore, researchers have developed large-range system calibration methods that use a polynomial model instead of a pinhole mode [180], separating the intrinsic and extrinsic parameter calibration processes [181,182].

As of today, basic FPP system calibration can be easily carried out. Yet, to our knowledge, it is still not easy to achieve consistently high calibration accuracy for inexpensive systems.

### 2.6. High speed realization

To capture highly dynamic scenes, both fringe projection and camera capture speeds must be high. The single fringe pattern projection methods can achieve highest possible speed (i.e., as fast as the camera captures). The single fringe pattern can be a static monochromatic pattern that is projected by a monochromatic projection unit and captured by an image acquisition unit. Then the single pattern fringe analysis technique is employed to recover wrapped phase, a spatial phase unwrapping method is used to unwrap phase, and then the unwrapped phase is used to recover 3D shape. This technique has been demonstrated successful in capturing extremely rapidly changing phenomena [16,17]. If the single static pattern is a colorful pattern, each color channel can encode different patterns. In such a case, the color pattern is projected by a color projection unit and a color camera is used to capture the color pattern for 3D imaging. Since only one single shot is required to capture 3D shape space [15], such a method could also achieve the speed of the camera. However, it might be challenging for this method to measure colorful objects with high quality. Furthermore, for color fringe projection, the digital light processing (DLP) technology usually cannot achieve comparable speed as those liquid crystal display (LCD) projection [183], or slider/grating projection technique [31] because of its inherent pattern generation nature [184]. Note that it typically requires the use of a high-speed camera to capture rapidly changing scenes without motion introduced errors. However, Zhang et al. [185] developed a single-shot method that permits the use of a relatively slower speed camera for high-speed motion capture by using a strobe light illumination. As discussed above, the single pattern analysis technique has several limitations that dual pattern methods can overcome.

Because using color fringe patterns is not desirable for measuring colorful objects [186], the multiple grayscale patterns have to be changed

rapidly, i.e., the projection unit has to switch one pattern to another at a high speed. Digital video projection technologies (e.g., LCD or DLP) were initially employed because it can produce images at a video rate (e.g., 60 Hz), and the achievable 3D imaging speed is a fraction of the projection speed. For example, assuming the camera speed is high enough, the maximum achievable 3D imaging speed is 20 Hz if a three-step phase-shifting algorithm is employed. Unlike LCD projection, DLP projects red, green, and blue channels sequentially, this unique projection technology enables higher measurement speed: achieving the video rate if a three-step phase-shifting algorithm is used (i.e., 60 Hz for a 60 Hz DLP projector). However, the major challenges for someone to use a DLP projector for high-speed and high-accuracy 3D imaging are: 1) DLP works off the time modulation to generate grayscale images [187], and thus synchronizing the projector and the camera becomes extremely important to properly capture the desired fringe images used for high-quality 3D imaging; 2) commercial DLP projector produces color image, and how to get rid of color becomes vital; and 3) the projection is nonlinear to accommodate human perception and thus compensating error caused by nonlinear effect is equally important for high accuracy measurement. Zhang and Huang [188] developed a 40 Hz system (due to the limitation of camera speed) using a DLP projector by successfully overcoming these challenges. Later on, Zhang et al. [79] developed a system that achieved 60 Hz 3D imaging rate using a DLP projector.

The DLP projector modulates the grayscale values by properly tilting each mirror either into (ON) or away (OFF) from the optical path at a rapid speed, and the ON and OFF timing ratio represents the grayscale value of a pixel [187]. The DLP projector actually switches light ON and OFF at a much higher rate than the video rate. Therefore, if binary patterns can be used, a higher 3D imaging speed can be achieved. As such, Zhang and Lei [33] developed the binary defocusing technique that generates by pseudo sinusoidal fringe patterns by defocusing binary patterns. The binary defocusing technique enables 3D imaging speed breakthrough by pairing with a high-speed 2D camera. For example, Zhang et al. [189] developed a 3D imaging system that achieved 667 Hz with a three-step phase-shifting algorithm and a DLP Discovery Development kit. Gong and Zhang [190] achieved 4,000 Hz rate by using a commercial DLP projector, Li et al. [191] achieved 5 kHz with a modified Fourier transform algorithm, and Zuo et al. [192] achieved 10 kHz with a modified Fourier transform algorithm.

Even though high-end DLP projection platform can switch binary patterns at up to 32 kHz, performing 3D imaging with such high rate rate is limited to small scale because the output light intensity is not sufficient to illuminate a large area. Since binary patterns can be used to produce sinusoidal fringe patterns, the pattern generation technique does not have to be computer generated, a mechanical projection system can be used. As such, researchers have developed mechanically spinning wheels to produce fringe patterns for 3D imaging [9,10]. By properly synchronizing the mechanical projector with cameras, precisely phase-shifted fringe patterns were also generated for high-quality 3D imaging. Hyun et al. [10] developed a system that can achieve up to 10 kHz 3D imaging rate regardless of the number of steps used for a phase-shifting algorithm. Comparing with DLP projection based 3D imaging system, the mechanical projection based 3D imaging system has the following merits: 1) the mechanical projection based 3D imaging system allows simultaneously achieving high speed and high quality assuming that the camera speed is high enough, whilst the DLP projection based 3D imaging system has to sacrifice quality for speed; 2) the mechanical projector allows the use of higher power light sources since the materials used to make the disk does not have to be Silicon; and 3) the mechanical projector can use a wider range spectrum of light than silicon-based DLP projector. Therefore, this technique could broaden the application of 3D imaging technology.

Researchers has also attempted to achieve high-speed 3D imaging by using an LED array for fringe pattern generation [11,12]. Since LED can turn on and off rapidly (tens of ns), this technology could switch fringe patterns at 100 kHz. The polarization camera was invented and has also been employed for high-speed 3D imaging because a single sensor can simultaneously capture four phase-shifted fringe patterns [193], albeit such a method is only applicable to those objects whose surface optical property preserves the polarization state of illumination light. Yet, another attempt was attempted to use fiber optics to generate interference fringe patterns, and using a phase modulator to create phase-shifting, such a technology could potentially achieve 3D imaging at GHz [194]. In general, more advanced hardware technologies create new opportunities for high speed 3D imaging, and thus 3D imaging field will grow with other fields.

Thus far, we only discussed fringe generation and acquisition speed, and have not mentioned about 3D optical information processing (e.g., 3D reconstruction, visualization, information analysis, and storage). Since the readers of this journal have the background of optics, we will not thoroughly cover other aspects in details. This does not mean that they are not critical. In fact, high-speed 3D optical information processing becomes increasingly critical because advanced 3D imaging methods have started being integrated into the *solution* system as a sensor. Due to the high computational cost, the state-of-the-art high-resolution real-time 3D information processing still requires massively parallel processors [195,196] such as grid computing, Graphics Processing Unit(GPUs) [91,197–200], Field Programmable Gate Arrays (FPGAs) [201,202], Advanced RISC Machines (ARMs), as well as cloud computing.

### 2.7. High dynamic range (HDR) techniques

To capture images of high-contract objects, high-dynamic range (HDR) techniques have been developed and employed in 2D imaging. Similarly, 3D HDR techniques have been explored, albeit they are not as mature as the 2D counterparts. The state-of-the-art HDR techniques either 1) blindly capture multiple exposures without the knowledge of the object to be measured [203–216], and 2) adjust the hardware settings (e.g., camera exposure time, projector brightness) to capture images after understanding object surface properties [205,217–228]. All these HDR methods coincidentally took advantage of pixel-by-pixel measurement of fringe analysis methods. Methods in the first category can capture data rapidly yet may not be optimized. In contrast, techniques belonging to the second category are accurate yet slow in terms of the optimization process because they capture a sequence of images, and analyze these images to determine the optimal conditions for high-quality measurement. Feng et al. [229] further categorized the major methods into camera-based techniques [203,204,207,210–216,222], projector-based techniques [205,206,208,217–219,223,226–228,230], adding equipment-based techniques [209,225,231], and hybrid techniques [220,221,224,232]. Despite these efforts, there are still a lack of methods for a standard fringe projection system to achieve HDR rapidly and robustly for dynamically changing scenes.

### 2.8. Representative applications

3D imaging, after all, as a sensing method whose value is limited without solving practical application problems. The state-of-the-art 3D imaging technologies based on FPP have benefited scientific discoveries and engineering practices. For example, in the cardiac mechanics field, Laughner et al. [233] employed a superfast FPP technique to capture the beating process of the heart, and further analyze the mechanical behavior of the heart; in the robotics field, FPP techniques have been used for navigation as well as manipulations [234–237]; in the law enforcement field, researchers have developed a portable and fully automated 3D imaging system for law enforcement personnel to collect evidence in the crime scene; and in the entertainment field, a rock band has employed a real-time 3D imaging technology [79] to capture the singing process; along with many other successful applications. Note that we do not intend to exhaustively cover all possible applications that FPP techniques have been used, but rather to show some successful examples over the past decades. We hope that by showing these diverse use

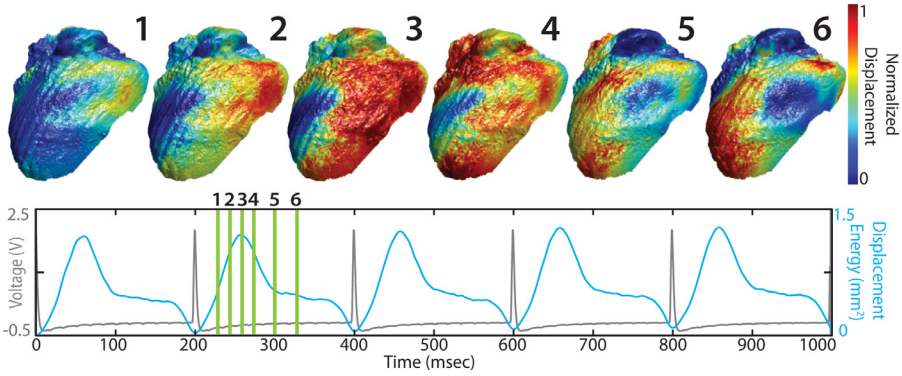


**Fig. 3.** Analysis of motion in the beating rabbit heart for apical pacing (CL = 200 ms) [233]. Location of each frame is indicated by green bars on a simultaneously recorded ECG (gray). Displacement energy (blue), a measure of total tissue displacement, is overlaid on each respective ECG.

cases, readers can be inspired to think about using FPP techniques for their own practical applications.

### 2.8.1. Cardiac mechanics

Over the last several decades, significant progress in cardiac electrophysiology has been made due to advances in optical methods of recordings of membrane potential, calcium transients and other parameters. Sophisticated optical mapping systems and fluorescent probes have been developed and applied to a wide range of applications. However, several limitations of biophotonic methodology hampered its application in both basic and clinical cardiac electrophysiology laboratory. One of the most significant limitations is a result of mechanical contractions of the heart, which cause a significant distortion in optical signals, making fluorescent recordings impossible in vivo and difficult in vitro. This long-standing problem of cardiovascular physiology could be solved by developing a synergistic approach to optically image metabolism and excitation-contraction coupling in a beating heart.

Laughner et al. [233] have carried out some preliminary study using the superfast FPP technology [90] to measure the dynamics of a beating rabbit heart and further analyzed cardiac displacement during ventricular pacing at CL = 200 ms. Fig. 3 shows the result. In this preliminary study, the 3D images were captured at 667 Hz rate, and the spatial resolution is approximately 87 μm with a total of 576 × 576 measurement points per 3D frame. They adapted the multi-frame geometric registration approach [238,239], that uses a state-of-the-art deformation model for estimating dense correspondences between frames. The preliminary study demonstrated the potential of utilizing the superfast 3D imaging technique to determine cardiac mechanics without any fiducial markers.

### 2.8.2. Robotics

There are two basic functions of a robot: mobility and manipulation, with both heavily relying on the perception of surrounding environment and the manipulated object, albeit other sensing forms (e.g., force) and control algorithms also play critical roles.

For an autonomous mobile robot, it is always desirable to accurately reconstruct 3D environment for efficient and precise navigation, and FPP techniques have been successfully applied in this field. For a urban search and rescue robot, Zhang et al. [234] developed a FPP sensor to reconstruct high-resolution 3D unknown/unstructured environment in real time; to allow the robot having different views of a landscape for obstacle avoidance, Xu et al. [235] developed a multi-directional FPP sensor to achieve large field of view (FOV) perception, and Wang et al. [240] designed an omnidirectional FPP sensor to achieve FOV of 360 degrees.

For an automatic manipulation robot, the end-effector is usually moved to a desired pose (position and orientation) through a vision-based control method. Comparing with other perception means, the high-accuracy merits of FPP techniques have seen it strengthen. Recently, several FPP-based visual servoing control methods are developed to perform accurate and robust pose adjustment of end-effector, especially for texture-less manipulated object where it is difficult to use a traditional passive vision for sensing. Xu et al. [236] demonstrated that the robot movement can be controlled by the 3D reconstructed point cloud from a FPP technique. Instead of using 3D point clouds, Rao et al. [237] further demonstrated that the robot movement can be directly controlled by the 2D phase map. With a FPP perception technique, the end-effector of an industrial robot can be adjusted to be perpendicular to a planar surface [241], a cylindrical surface [242], or a free-form surface [237].

Fig. 4 shows a robotic drilling system that is composed of a robot manipulator (Model: ABB 4600), a drilling device and a FPP system we developed. This drilling system can drill on a free-form surface accurately by virtue of measurement from the FPP system. Instead of using the reconstructed 3D point clouds for the drilling normal adjustment process, the 2D phase map obtained from FPP system is taken as visual features to synthesize the visual servoing control law. Thus the orientation of the drilling device can be adjusted iteratively to align with the real normal direction on the free-form surface accurately and robustly directly from the phase without reconstructing 3D points. This phase-based control strategy is more efficient computationally than the 3D geometry based control strategy.

## 2.9. Crime scene evidence collection

The Forensic Science Research and Development Technology Working Group (TWG) was tasked by the National Institute of Justice (NIJ) with identifying and prioritizing R&D to satisfy operational requirements for forensic science disciplines. In the field of Impression & Pattern/Trace Evidence, the TWG identified the operation needs in “Novel and/or improved evidence recognition, collection, and visualization tools and analytical instrumentation for field and lab use” [243]. In March 2016, National Institute of Standards and Technology (NIST) published a report on the research need in the field of Testing and Validation of 3D Imaging Technologies for Footwear and Tire Impressions Evidence, the report assessed that “(there is a) major gap in current knowledge and no or limited current research is being conducted” [244].

To fill the technological gap, a researcher team has developed a fully-automated 3D imaging system that allows the user easily and quickly capture high-resolution shoe and tire impressions. The hardware was designed to be portable and easy to setup; and the software graphical user interface (GUI) was designed to be intuitive and thus users do not need training for operation. The prototype system we have developed is portable and can be packed into Pelican 1450 Case (interior dimension 14.62″ × 10.18″ × 6.00″). Fig. 5(a) shows the prototype system. The system can be set up quickly with four steps for data capture: 1) plug in the power cord; 2) connect the USB cable between the device and a laptop computer; 3) toggle the power switch on; and 4) start the software for data capture. Fig. 5(b) shows the software GUI to operate our prototype system. The software was designed to be intuitive and fully automated such that no training is necessary to operate our prototype

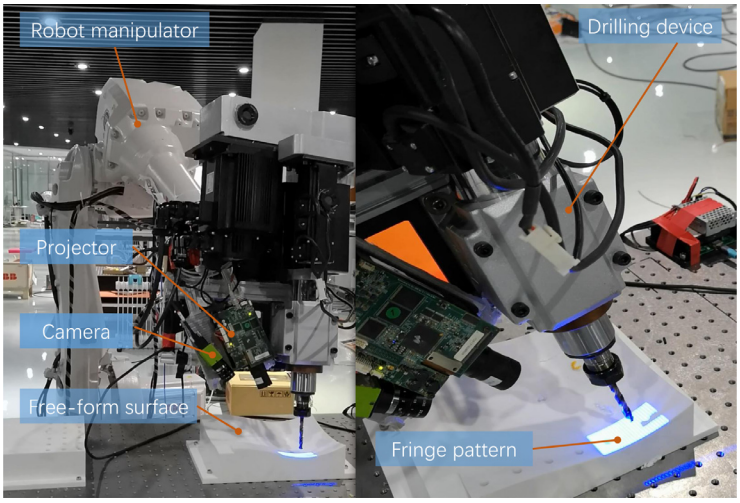


**Fig. 4.** A robotic drilling system with a FPP system as the visual sensor: the phase-map-based visual servoing control law is synthesized based on the phase map obtained from a FPP sensor without reconstructing 3D points.

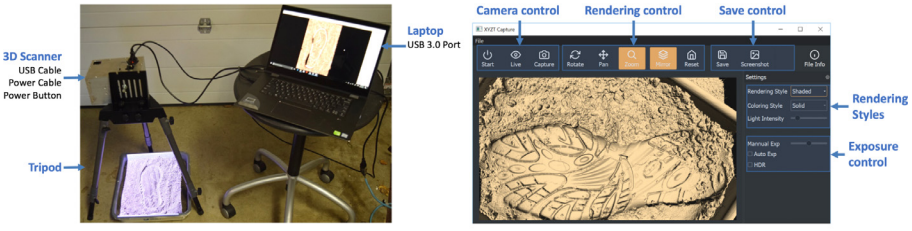


(a) (b)

**Fig. 5.** Portable 3D imaging prototype for crime scene documentation. (a) Hardware system; (b) software graphical user interface (GUI).

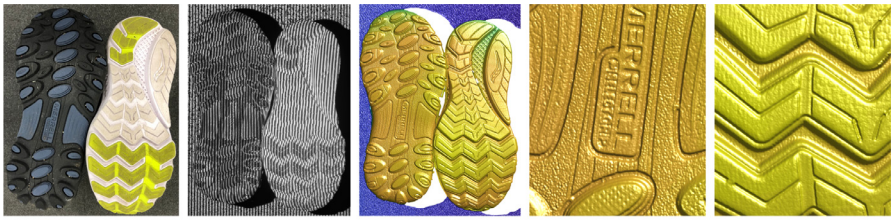

(a) (b) (c) (d) (e)

**Fig. 6.** Measurement result of high contrast scene with and without HDR technique. (a) Photograph of the high-contrast scene; (b) one of the fringe patterns using the HDR technique; (c) 3D result by automatically optimizing the HDR exposure times; (d) closeup view of the 3D results for a small region on the left shoe; (e) closeup view of the 3D results for a small region on the right shoe.

system. The prototype system were evaluated various forensic examiners in the United States and none of whom has difficulty figuring out how to use the system without user instructions.

The fully automated HDR algorithms were also evaluated by experimentally measuring a high-contrast scene shown in Fig. 6(a). The scene includes two shoes and a black background: the level of brightness varies drastically across the entire scene. For such a scene, a single exposure can only ensure one shoe is measured with a high quality. Fig. 6(b) shows one of the combined fringe patterns, and Fig. 6(c) shows the corresponding 3D result. Once again, Fig. 6(d) and Fig. 6(e) respectively shows the zoom-in views of the left shoe and for the right shoe. Both shoes are measured with high quality.

Fig. 7 shows the results of measuring footwear and tire impressions in fine soils by forensic examiners. They all showed great success of capturing critical evidence artifacts that are difficult for conventional casting.

### 2.10. Music video

By integrating songs with visual imagery to produce short films, the entertainment industry produces music videos to promote songs or present artistic visuals. Even at the current world, music videos are primarily created in 2D as a media for consumers. As a result, it is not easy for a non professionalist to edit visuals to fit his/her own tastes. Radiohead, an English rock band, pioneered the concept of producing 3D music videos. Once 3D visuals are recorded, the music videos can be altered at any given stage, and even by the consumers. They employed the real-time FPP technique [79] to record the dynamic singing process in details, as well the LIDAR technology to digitize the scene [245]. One of the final rendering of the 3D videos is produced a conventional 2D music video [246]. The same visual recording was also used to produce different 2D videos [247,248]. Fig. 8 shows some of the video frame with different visual effects.

## 3. Challenges

Despite the advancements of FPP technologies, challenges still remain for the state-of-the-art FPP techniques to solve practical application problems. This section provides some representative examples that FPP techniques are highly valuable yet not ready at this point. We believe that 3D imaging experts and application area domain experts have to seamless work together to solve such very challenging problems in those fields.

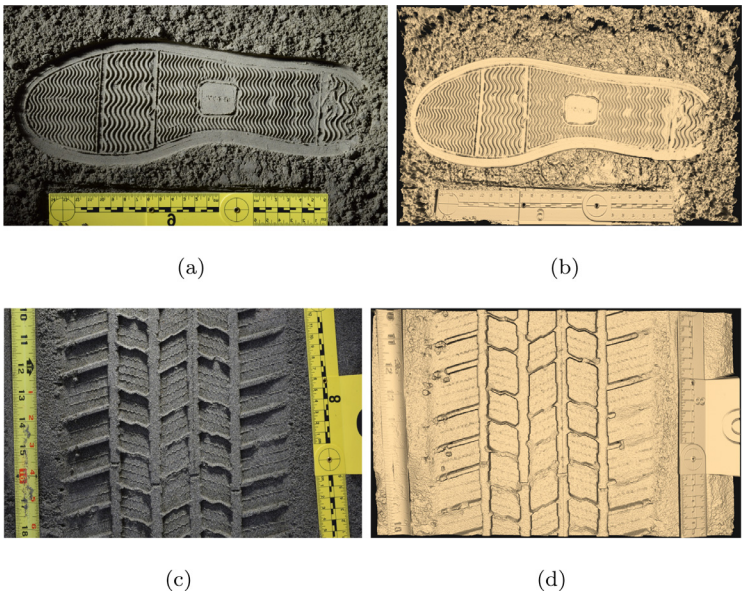

**Fig. 7.** Measurement results of impressions in fine soil. (a) 2D image of footwear impression; (b) 3D results of the footwear impression; (c) 2D image of tire impression; (d) 3D results of the tire impression.

**Fig. 8.** Visual effects generated by recording 3D video of "House of Cards" by Radiohead. (a) One of the 2D music video frames created by Radiohead [246]; (b) one of the 2D music video frames created by one user [247]; (c) one of the 2D video frames created by another user [248].

Let us take a look at the robotics application once again. Domestic robots are in a huge and rapidly increasing demand for the aging society. However, the state-of-the-art domestic robots are still in a preliminary level and not capable of advanced tasks in real-life scenarios, due to the fact that the 3D sensing techniques currently employed in such robots lack intelligence and cannot adapt to complex tasks. Consider the service robot as an example, in order to clean and arrange the room, the robot should first be able to map the entire room and locate itself in real time for the layout changes dynamically. However, current FPP or other 3D sensing techniques aim to reconstruct the whole scene in an unified resolution, which is time-consuming and unnecessary, since some parts of the scene are not important and could be processed more efficiently. For instance, the wall could be treated as a simple plane for indoor navigation, while the objects on the table should be reconstructed more accurately for robotic interaction. After the mapping, the robot are expected to recognize and locate target objects that vary in size, shape, materials and textures. For example, there are glass cups, steel forks, ceramic bowels, and black tablecloth on a table. However, at the current stage, real-time FPP techniques cannot obtain accurate and complete geometry information for objects with challenging optical properties (e.g., darkness, transparency, specularity). The incomplete and noisy geometry information limits its application in robot grasping and manipulation, which is fundamental for most real-life robotic tasks. Moreover, compared with FPP with a fixed viewpoint and field of view, human can change the viewpoint and focal area dynamically during the interaction with objects, which allows human to collect critical feedback information for more precise interaction. Such attention mechanism could be a promising direction for future FPP development, including proactive viewpoint adjustment, FOV adaptation, as well as self-recalibration.

Another application that FPP could play a critical role but not yet is Additive Manufacturing (AM). AM, also called 3D printing, is a process of depositing material layer by layer to form a 3D object. Hence, it is a promising manufacturing mode in complex geometry and material saving. However, the quality and repeatability of the object manufactured by AM are still a challenging issue due to the high sensibility of the process parameters [249]. Therefore, 3D measurement is critical to asses the geometric feature and detect defect during the forming process. Compared with the post-process measurement after the object has been manufactured, the in-situ measurement can inspect the internal and obscured structure, increase throughput by adjusting the manufacturing process through feedback control, and/or to reduce waste by stopping manufacturing faulted product during the process. FPP holds the advantageous features such as non-contact, high speed, high resolution, and high accuracy; and thus is applicable for in-situ measurement in AM [250]. In fact, attempts have been made in recent years. For example, in the laser powder bed fusion additive process, FPP has been used to measure height profile and surface topography of sintered powder in each layer for quality control [251–254]. To avoid the error propagation and defect along the layer, FPP is used to optimize process parameter (distance between nozzle and substrates) in laser metal deposition[255]. Despite the fact that FPP has been increasingly studied in AM, the state-of-the-art techniques only perform measurements when the deposition stops, limiting the manufacturing efficiency. Furthermore, the current practice might not replicate the true AM process when the deposition continuously moving. In addition, currently, the process parameters of the current layer is only optimized from the measurement of the last sintered layer due to the bright and specular melt pool, heat radiation, and spark noise. Therefore, in order to achieve in-situ measurements for AM, the measurements have to be performed without stopping the de-

position, information analysis has to be accomplished instantaneously without slowing down the manufacturing process, and the 3D sensing system has to be integrated into the AM machines instead of a separate instrument to close the manufacturing process loop. All these pose challenges to the current FPP techniques.

Even though these two examples presented here are distinct in nature, they all reached the limitations of the existing 3D sensing techniques and thus need for better sensors in terms of power consumption, miniaturization, more adaptive environment, self-calibration and more robustness, along with better data processing algorithms for more seamless integration of sensing and systems into a total solution package. There are some common needs in sensing technology itself to address these challenges. They are 1) automation in 3D FPP techniques without any user input (e.g., auto focus, auto exposure; 2) adaptive techniques for varying scenes (e.g., dark surface, bright surface); 3) smartness for intelligent information extraction (e.g., noise filtering); 4) robustness to survive harsh environments (e.g., strong lighting, system vibration, air turbulence); and 5) self-recovery for the loss of calibration (e.g., focal length change due to temperature, geometric relationship change due to vibration).

Of course, these challenges lead to the future research opportunities for researchers in the field as well as other disciplines.

## 4. Future perspectives

Despite the challenges still being faced in this field, the future of 3D imaging based on FPP techniques is promising because large strides have been and will continue to be made in the field. Being more integrated parts of every day lives, high-accuracy 3D imaging technologies based on FPP could conquer even more challenging societal issues such as more natural daily communications (e.g., 3D Facetime with VR/AR technologies), homeland security (e.g., fighting with crime), healthcare (e.g., telemedicine, vision guided robotic surgeries), natural disaster reliefs (e.g., search and rescue after earthquake), human-machine interface (e.g., service robots for the elderly), unstructured environment understanding (e.g., space exploration), along with many others.

3D imaging technologies adopted in the daily lives so far are simple with low accuracy. However, FPP techniques can be the future because of their advantageous features such as speed and accuracy. The fundamental challenges are 1) to achieve cost-effective fabrication; 2) to reduce the physical footprint for embedded applications; 3) to develop robust yet adaptive algorithms for unknown scenes; and 4) to develop fully automated and accurate self-calibration methods.

The rapidly exploding AI technologies will be leveraged to advance 3D imaging technologies based on FPP. We believe that AI could 1) broaden the adoption 3D imaging technologies in areas that have never been used before; 2) sparkle new ideas to solve the long-standing problems in the FPP field (e.g., phase unwrapping, 3D reconstruction, noise impact reduction); and 3) propel the development of complete “solution” systems for a specific application.

The robotics field, by itself, is positioned to solve numerous challenging problems. Yet, most intelligent robotics still use “baby” 3D sensors as the main perception means. Advanced more accurate 3D sensors such as those based on FPP techniques, if employed, could significantly simplify many difficult problems in the field (e.g., grasping, precision navigation). As discussed before, the 3D sensing needs in the robotics field cannot be met in the current 3D sensing field, and thus the robotics field could further drive technological developments in the 3D sensing field.

Additive manufacturing (AM) is still a growing field that could transform the manufacturing industry at large. As discussed before, quality control remains one of the grand challenges. In the AM field, sensing will be an integrated parts of the “solution” system: in-situ sensing, data analytics, control, material processing, etc, have to seamlessly work together to produce consistently high-quality products. Therefore, this field could be one of the exemplary areas that promote interdisciplinary collaborations since domain experts from many distinct disciplines must work together to conquer those grand challenges facing in the field.

3D information processing could grow to be a vibrant field that spans from 3D data/video storage, 3D data/video compression, 3D data/video information analysis, along with 3D data/video communication.

The FPP society, as a whole, will grow rapidly propelled by the availability of consumer level 3D sensors, the increasing acceptance of the general public, the ever growing needs in applications, along with the incoming software/hardware tools available to the community.

## 5. Summary

This paper presented our opinions on the current status of fringe projection profilometry (FPP) techniques, challenges that the FPP field is still facing, and the future perspectives that FPP could lead to. This paper serves as a reference for students, researchers, engineers, and practitioners to learn where the field stands. However, our opinions might not be accurate, due to our limited knowledge and expertise. Therefore, we encourage all readers to think critically about our thoughts, challenge what we presented, and contribute the advancement of this exciting field.

## Acknowledgments

We would like to thank the current and former collaborators, students, as well friends who made significant contributions to the FPP field. It was their tremendous effort to make this field vibrant and exciting. We also would like to thank our sponsors to support our study in the field of FPP, and our explorations in application areas. Last but not the least, we would like to thank Professor Pramod Rastogi for his invitation and his faith in us to work on this paper. Professor Song Zhang especially thanks the constant support and genuine guidance that Professor Rastogi offered to Prof. Zhang for his career advancement over the past decade.

This work were partially supported by National Science Foundation under grant numbers CMMII-1531048, CMMII-1523048, and IIS-1637961, National Institute of Justice (NIJ) under the grant number 2016-DN-BX-0189, and the National Natural Science Foundation of China (NSFC) under grant numbers U1613205 and 51675291. The views expressed in this paper are those of the authors and not necessarily those of the sponsors (NSF, NIJ, NSFC).

## Supplementary material

Supplementary material associated with this article can be found, in the online version, at 10.1016/j.optlaseng.2020.106193

## References

[1] Dhond UR, Aggarwal JK. Structure from stereo-a review. IEEE Trans Systems, Man and Cybernetics 1989;19(6):1489–510.
[2] Lazaros N, Sirakoulis GC, Gasteratos A. Review of stereo vision algorithms: from software to hardware. Int J Optomechatronics 2008;2(4):435–62.
[3] Li B, An Y, Cappelleri D, Xu J, Zhang S. High-accuracy, high-speed 3D structured light imaging techniques and potential applications to intelligent robotics. Int J Intell Robotic Appl 2017;1(1):86–103.
[4] Hansard M, Lee S, Choi O, Horaud RP. Time-of-Flight cameras. Springer-Verlag London; 2013.
[5] Huang Y, Shang Y, Liu Y, Bao H. Handbook of 3D Machine Vision: Optical Metrology and Imaging. 1st. CRC; 2013. p. 33–56.
[6] Salvi J, Fernandez S, Pribanic T, Llado X. A state of the art in structured light patterns for surface profilometry. Patt Recogn 2010;43(8):2666–80.
[7] Zhang S. High-speed 3D shape measurement with structured light methods: a review. Opt Laser Eng 2018;106:119–31.
[8] Schaffer M, Große M, Harendt B, Kowarschik R. Coherent two-beam interference fringe projection for high-speed three-dimensional shape measurements. Appl Opt 2013;52(11):2306–11.
[9] Heist S, Lutzke P, Schmidt I, Dietrich P, Kühmstedt P, Tünnermann A, et al. High-speed three-dimensional shape measurement using gobo projection. Opt Laser Eng 2016;87:90–6.
[10] Hyun J-S, Chiu GT-C, Zhang S. High-speed and high-accuracy 3D surface measurement using a mechanical projector. Opt Express 2018;26(2):1474–87.

[11] Heist S, Mann A, Kühmstedt P, Schreiber P, Notni G. Array projection of aperiodic sinusoidal fringes for high-speed three-dimensional shape measurement. Opt Eng 2014;53(11):112208.
[12] Fujigaki M, Oura Y, Asai D, Murata Y. High-speed height measurement by a light-source-stepping method using a linear led array. Opt Express 2013;21(20):23169–80.
[13] Zhang S. Recent progresses on real-time 3-d shape measurement using digital fringe projection techniques. Opt Laser Eng 2010;48(2):149–58.
[14] der Jeught SV, Dirckx JJ. Real-time structured light profilometry: a review. Opt Laser Eng 2016;87:18–31.
[15] Zhang Z. Review of single-shot 3D shape measurement by phase calculation-based fringe projection techniques. Opt Laser Eng 2012;50(8):1097–106.
[16] Takeda M. Fourier fringe analysis and its applications to metrology of extreme physical phenomena: a review. Appl Opt 2013;52(1):20–9.
[17] Su X, Zhang Q. Dynamic 3-d shape measurement method: a review. Opt Laser Eng 2010;48:191–204.
[18] Geng J. Structured-light 3D surface imaging: a tutorial. Adv Opt Photonic 2011;3(2):128–60.
[19] Zuo C, Feng S, Huang L, Tao T, Yin W, Chen Q. Phase shifting algorithms for fringe projection profilometry: a review. Opt Laser Eng 2018;109:23–59.
[20] Scharstein D, Szeliski R. A taxonomy and evaluation of dense two-frame stereo correspondence algorithms. Intl J Comp Vis 2002;47(1–3):7–42.
[21] Hartley RI, Zisserman A. Multiple view geometry in computer vision. Cambridge University Press, ISBN: 0521623049; 2000.
[22] Rusinkiewicz S, Hall-Holt O, Levoy M. Real-time 3D model acquisition. ACM Trans Graph 2002;21(3):438–46.
[23] Hall-Holt O, Rusinkiewicz S. Stripe boundary codes for real-time structured-light range scanning of moving objects. In: The 8th IEEE International Conference on Computer Vision; 2001. II:359–366.
[24] Pan J, Huang PS, Chiang F-P. Color-coded binary fringe projection technique for 3-d shape measurement. Opt Eng 2005;44(2):023606.
[25] Pan J, Huang P, Zhang S, Chiang F-P. Color n-ary gray code for 3-d shape measurement. In: Proc. 12th Int'l Conference on Experimental Mechanics; 2004.
[26] Davis J, Ramamoorthi R, Rusinkiewicz S. Spacetime stereo: a unifying framework for depth from triangulation. In: Proc. of IEEE Conference on computer vision and pattern recognition, 2; 2003. II:359-366.
[27] Zhang L, Curless B, Seitz S. Spacetime stereo: Shape recovery for dynamic scenes. In: Proc. Comp. Vis. Patt. Recogn.; 2003. p. 367–74.
[28] Zhang L, Snavely N, Curless B, Seitz SM. Spacetime faces: high-resolution capture for modeling and animation. ACM Trans Graph 2004;23(3):548–58.
[29] Hariharan P. Basics of interferometry. Academic Press; 2006.
[30] Anderson JA, Porter RW. Ronchi's method of optical tesing. Astrophys J 1929;70:175–81.
[31] Wust C, Capson DW. Surface profile measurement using color fringe projection. Mach Vis Appl 1991;4:193–203.
[32] Rowe SH, Welford WT. Surface topography of non-optical surfaces by projected interference fringes. Nature 1967;216(5117):786–7.
[33] Lei S, Zhang S. Flexible 3-d shape measurement using projector defocusing. Opt Lett 2009;34(20):3080–2.
[34] Wang Y, Zhang S. Optimal pulse width modulation for sinusoidal fringe generation with projector defocusing. Opt Lett 2010;35(24):4121–3.
[35] Ayubi GA, Ayubi JA, Martino JMD, Ferrari JA. Pulse-width modulation in defocused 3-d fringe projection. Opt Lett 2010;35:3682–4.
[36] Zuo C, Chen Q, Feng S, Feng F, Gu G, Sui X. Optimized pulse width modulation pattern strategy for three-dimensional profilometry with projector defocusing. Appl Opt 2012;51(19):4477–90.
[37] Wang Y, Zhang S. Three-dimensional shape measurement with binary dithered patterns. Appl Opt 2012;51(27):6631–6.
[38] Dai J, Li B, Zhang S. High-quality fringe patterns generation using binary pattern optimization through symmetry and periodicity. Opt Laser Eng 2014;52:195–200.
[39] Lohry W, Zhang S. Genetic method to optimize binary dithering technique for high--quality fringe generation. Opt Lett 2013;38(4):540–2.
[40] Sun J, Zuo C, Feng S, Yu S, Zhang Y, Chen Q. Improved intensity-optimized dithering technique for 3D shape measurement. Opt Laser Eng 2015;66:158–64.
[41] Li X-X, Zhang Z-J. High-quality fringe pattern generation based on binary pattern optimization with projector defocusing. J Opt Technol 2017;84(1):22–8.
[42] Xiao Y, Li Y. High-quality binary fringe generation via joint optimization on intensity and phase. Opt Laser Eng 2017;97:19–26.
[43] Lu F, Wu C, Yang J. Optimized dithering technique for three-dimensional shape measurement with projector defocusing. Opt Commun 2019;430:246–55.
[44] Xu Z-X, Chan Y-H, Lun DP. High-quality octa-level fringe pattern generation for improving the noise characteristics of measured depth maps. Opt Lasers Eng 2017;98:99–106.
[45] Zuo C, Chen Q, Gu G, Feng S, Feng F, Li R, et al. High-speed three-dimensional shape measurement for dynamic scenes using bi-frequency tripolar pulse-width–modulation fringe projection. Opt Laser Eng 2013;51(8):953–60.
[46] Silva A, Flores JL, Munoz A, Ayubi GA, Ferrari JA. Three-dimensional shape profiling by out-of-focus projection of colored pulse width modulation fringe patterns. Appl Opt 2017;56(18):5198–203.
[47] Ajubi GA, Ayubi JA, Martino JMD, Ferrari JA. Three-dimensional profiling with binary fringes using phase-shifting interferometry algorithms. Appl Opt 2011;50(2):147–54.
[48] Zhu J, Zhou P, Su X, You Z. Accurate and fast 3D surface measurement with temporal-spatial binary encoding structured illumination. Opt Express 2016;24(25):28549–60.
[49] Wang Y, Jiang C, Zhang S. Double-pattern triangular pulse width modulation technique for high-accuracy high-speed 3D shape measurement. Opt Express 2017;25(24):30177–88.
[50] Takeda M, Mutoh K. Fourier transform profilometry for the automatic measurement of 3-d object shapes. Appl Opt 1983;22:3977–82.
[51] Kemao Q. Windowed fourier transform for fringe pattern analysis. Appl Opt 2004;43:2695–702.
[52] Kemao Q. Two-dimensional windowed fourier transform for fringe pattern analysis: principles, applications and implementations. Opt Laser Eng 2007;45:304–17.
[53] Qian K. Comparison of fourier transform, windowed fourier transform, and wavelet transform methods for phase extraction from a single fringe pattern in fringe projection profilometry. Opt Laser Eng 2010;48(2):141–8.
[54] Qian K. Applications of windowed fourier fringe analysis in optical measurement: a review. Opt Laser Eng 2015;66:67–73.
[55] Zhong J, Zeng H. Multiscale windowed fourier transform for phase extraction of fringe patterns. Appl Opt 2007;46(14):2670–5.
[56] Gdeisat MA, Burton DR, Lalor MJ. Spatial carrier fringe pattern demodulation by use of a two-dimensional continuous wavelet transform. Appl Opt 2006;45(34):8722–32.
[57] Zhong J, Weng J. Spatial carrier-fringe pattern analysis by means of wavelet transform: wavelet transform profilometry. Appl Opt 2004;43(26):4993–8.
[58] Abid AZ, Gdeisat MA, Burton DR, Lalor MJ, Lilley F. Spatial fringe pattern analysis using the two-dimensional continuous wavelet transform employing a cost function. Appl Opt 2007;46(24):6120–6.
[59] Gdeisat MA, Burton DR, Lalor MJ. Spatial carrier fringe pattern demodulation by use of a two-dimensional continuous wavelet transform. Appl Opt 2006;45(34):8722–32.
[60] Gdeisat MA, Abid A, Burton DR, Lalor MJ, Lilley F, Moore C, et al. Spatial and temporal carrier fringe pattern demodulation using the one-dimensional continuous wavelet transform: recent progress, challenges, and suggested developments. Opt Lasers Eng 2009;47(12):1348–61.
[61] Trusiak M, Służewski Ł, Patorski K. Single shot fringe pattern phase demodulation using hilbert-huang transform aided by the principal component analysis. Opt Express 2016;24(4):4221–38.
[62] Gdeisat M, Burton D, Lilley F, Arevalillo-Herráez M. Fast fringe pattern phase demodulation using fir hilbert transformers. Opt Commun 2016;359:200–6.
[63] Chen W, Su X, Cao Y, Zhang Q, Xiang L. Method for eliminating zero spectrum in fourier transform profilometry. Opt Lasers Eng 2005;43(11):1267–76.
[64] Luo F, Chen W, Su X. Eliminating zero spectra in fourier transform profilometry by application of hilbert transform. Opt Commun 2016;365:76–85.
[65] Feng S, Zuo C, Yin W, Gu G, Chen Q. Micro deep learning profilometry for high--speed 3D surface imaging. Opt Lasers Eng 2019;121:416–27.
[66] der Jeught SV, Dirckx JJJ. Deep neural networks for single shot structured light profilometry. Opt Express 2019;27(12):17091–101.
[67] Guo L, Su X, Li J. Improved fourier transform profilometry for the automatic measurement of 3D object shapes. Opt Eng 1990;29(12):1439–44.
[68] Guo H, Huang PS. Absolute phase technique for the fourier transform method. Opt Eng 2009;48(2):043609.
[69] Zhang Q, Su X. High-speed optical measurement for the drumhead vibration. Opt Express 2005;13(8):3110–16.
[70] Li B, Zhang S. Superfast, high-resolution absolute 3D recovery of a stabilized flapping flight process. Opt Express 2017;25(22):27270–82.
[71] Zhang S, Yau S-T. High-speed three-dimensional shape measurement system using a modified two-plus-one phase-shifting algorithm. Opt Eng 2007;46(11):113603.
[72] Optical shop testing. Malacara D, editor. 3rd. New York, NY: John Wiley and Sons; 2007.
[73] Zhang S. Absolute phase retrieval methods for digital fringe projection profilometry: a review. Opt Laser Eng 2018;107:28–37.
[74] Two-Dimensional phase unwrapping: theory, algorithms, and software. Ghiglia DC, Pritt MD, editors. New York: John Wiley and Sons; 1998.
[75] Su X, Chen W. Reliability-guided phase unwrapping algorithm: a review. Opt Laser Eng 2004;42(3):245–61.
[76] Zhao M, Huang L, Zhang Q, Su X, Asundi A, Kemao Q. Quality-guided phase unwrapping technique: comparison of quality maps and guiding strategies. Appl Opt 2011;50(33):6214–24.
[77] Cruz-Santos W, Lopez-Garcia L. Implicit absolute phase retrieval in digital fringe projection without reference lines. Appl Opt 2015;54(7):1688–95.
[78] Guo H, Huang P. 3-d shape measurement by use of a modified fourier transform method. In: Proc. SPIE, 7066; 2008. p. 70660E.
[79] Zhang S, Yau S-T. High-resolution, real-time 3-d absolute coordinate measurement based on a phase-shifting method. Opt Express 2006;14(7):2644–9.
[80] Su X, Zhang Q, Xiao Y, Xiang L. Dynamic 3-d shape measurement techniques with marked fringes tracking. In: Fringe 2009; 2009. p. 493–6.
[81] Cui H, Liao W, Dai N, Cheng X. A flexible phase-shifting method with absolute phase marker retrieval. Measurement 2012;45(1):101–8.
[82] Xiao Y, Su X, Zhang Q, Li Z. 3-D profilometry for the impact process with marked fringes tracking. Opto-Electron Eng 2007;34(8):46–52.
[83] Budianto B, Lun P, Hsung T-C. Marker encoded fringe projection profilometry for efficient 3D model acquisition. Appl Opt 2014;53(31):7442–53.
[84] Cong P, Xiong Z, Zhang Y, Zhao S, Wu F. Accurate dynamic 3D sensing with fourier-assisted phase shifting. IEEE J Sel Top Signal Process 2015;9(3):396–408.
[85] Cheng Y-Y, Wyant JC. Two-wavelength phase shifting interferometry. Appl Opt 1984;23:4539–43.
[86] Cheng Y-Y, Wyant JC. Multiple-wavelength phase shifting interferometry. Appl Opt 1985;24:804–7.
[87] Wang Y, Zhang S. Superfast multifrequency phase-shifting technique with optimal pulse width modulation. Opt Express 2011;19(6):5143–8.

[88] Towers DP, Jones JDC, Towers CE. Optimum frequency selection in multi-frequency interferometry. Opt Lett 2003;28:1–3.
[89] Zuo C, Huan L, Zhang M, Chen Q, Asundi A. Temporal phase unwrapping algorithms for fringe projection profilometry: a comparative review. Opt Laser Eng 2016;85:84–103.
[90] Wang Y, Laughner JI, Efimov IR, Zhang S. 3D absolute shape measurement of live rabbit hearts with a superfast two-frequency phase-shifting technique. Opt Express 2013;21(5):5632–822.
[91] Karpinsky N, Hoke M, Chen V, Zhang S. High-resolution, real-time three--dimensional shape measurement on graphics processing unit. Opt Eng 2014;53(2):024105.
[92] Liu K, Wang Y, Lau DL, Hao Q, Hassebrook LG. Dual-frequency pattern scheme for high-speed 3-d shape measurement. Opt Express 2010;18:5229–44.
[93] Sansoni G, Carocci M, Rodella R. Three-dimensional vision based on a combination of gray-code and phase-shift light projection: analysis and compensation of the systematic errors. Appl Opt 1999;38:6565–73.
[94] Zhang S. Flexible 3D shape measurement using projector defocusing: extended measurement range. Opt Lett 2010;35(7):931–3.
[95] Wang Y, Zhang S, Oliver JH. 3-D shape measurement technique for multiple rapidly moving objects. Opt Express 2011;19(9):5149–55.
[96] Zhang Q, Su X, Xiang L, Sun X. 3-D shape measurement based on complementary gray-code light. Opt Laser Eng 2012;50:574–9.
[97] Wu Z, Zuo C, Guo W, Tao T, Zhang Q. High-speed three-dimensional shape measurement based on cyclic complementary gray-code light. Opt Express 2019;27(2):1283–97.
[98] Zheng D, Kemao Q, Da F, Seah HS. Ternary gray code-based phase unwrapping for 3D measurement using binary patterns with projector defocusing. Appl Opt 2017;56(13):3660–5.
[99] Li Y, Jin H, Wang H. Three-dimensional shape measurement using binary spatio-temporal encoded illumination. J Opt A, Pure Appl Opt 2009;11(7):075502.
[100] An Y, Zhang S. Three-dimensional absolute shape measurement by combining binary statistical pattern matching with phase-shifting methods. Appl Opt 2017;56(19):5418–26.
[101] Li J-L, Su H-J, Su X-Y. Two-frequency grating used in phase-measuring profilometry. Appl Opt 1997;11:277–80.
[102] Guan C, Hassebrook LG, Lau DL. Composite structured light pattern for three-dimensional video. Opt Express 2003;11:406–17.
[103] Zhang S. Composite phase-shifting algorithm for absolute phase measurement. Opt Laser Eng 2012;50(11):1538–41.
[104] Wang Y, Zhang S. Novel phase coding method for absolute phase retrieval. Opt Lett 2012;37(11):2067–9.
[105] Zhou C, Liu T, Si S, Xu J, Liu Y, Lei Z. Phase coding method for absolute phase retrieval with a large number of codewords. Opt Express 2012;20(22):24139–50.
[106] Zhou C, Liu T, Si S, Xu J, Liu Y, Lei Z. An improved stair phase encoding method for absolute phase retrieval. Opt Laser Eng 2015;66:269–78.
[107] Chen X, Lu C, Ma M, Mao X, Mei T. Color-coding and phase-shift method for absolute phase measurement. Opt Comm 2013;298:54–8.
[108] Xing Y, Quan C, Tay C. A modified phase-coding method for absolute phase retrieval. Opt Laser Eng 2016;87:97–102.
[109] Hyun J, Zhang S. Superfast 3D absolute shape measurement using five fringe patterns. Opt Laser Eng 2017;90:217–24.
[110] Zhong K, Li Z, Shi Y, Wang C, Lei Y. Fast phase measurement profilometry for arbitrary shape objects without phase unwrapping. Opt Lasers Eng 2013;51(11):1213–22.
[111] Li Z, Zhong K, Li Y, Zhou X, Shi Y. Multiview phase shifting: a full-resolution and high-speed 3D measurement framework for arbitrary shape dynamic objects. Opt Lett 2013;38(9):1389–91.
[112] Brauer-Burchardt C, Kuhmstedt P, Notni G. Phase unwrapping using geometric constraints for high-speed fringe projection based 3D measurements. In: Proc. SPIE, 8789; 2013. 878906.
[113] Ishiyama R, Sakamoto S, Tajima J, Okatani T, Deguchi K. Absolute phase measurements using geometric constraints between multiple cameras and projectors. Appl Opt 2007;46(17):3528–38.
[114] Brauer-Burchardt C, Kuhmstedt P, Heinze M, Kuhmstedt P, Notni G. Using geometric constraints to solve the point correspondence problem in fringe projection based 3D measuring systems. In: Proc. of the 16th international conference on Image analysis and processing, Part II; 2011. p. 265–74.
[115] Huddart YR, Valera JDR, Weston NJ, Moore AJM. Absolute phase measurement in fringe projection using multiple perspectives. Opt Express 2013;21(18):21119–30.
[116] Lohry W, Chen V, Zhang S. Absolute three-dimensional shape measurement using coded fringe patterns without phase unwrapping or projector calibration. Opt Express 2014;22(2):1287–301.
[117] Jiang C, Zhang S. Absolute phase unwrapping for dual-camera system without embedding statistical features. Opt Eng 2017;56(9):094114.
[118] An Y, Hyun J-S, Zhang S. Pixel-wise absolute phase unwrapping using geometric constraints of structured light system. Opt Express 2016;24(15):18445–59.
[119] Xing Y, Quan C. Reference-plane-based fast pixel-by-pixel absolute phase retrieval for height measurement. Appl Opt 2018;57(17):4901–8.
[120] Xing Y, Quan C. Enhanced reference-plane-based dual-frequency absolute phase retrieval for depth measurement. Meas Sci Technol 2018;29(10):105003.
[121] Deng H, Deng J, Ma M, Zhang J, Yao P, Yu L, et al. Direction-determined phase unwrapping using geometric constraint of the structured light system: the establishment of minimum phase map. Opt Commun 2017;402:14–19.
[122] Yin W, Zuo C, Feng S, Tao T, Hu Y, Huang L, et al. High-speed three-dimensional shape measurement using geometry-constraint-based number-theoretical phase unwrapping. Opt Lasers Eng 2019;115:21–31.
[123] Cheng T, Du Q, Jiang Y. Color fringe projection profilometry using geometric constraints. Opt Commun 2017;398:39–43.
[124] Li B, Bell T, Zhang S. Computer-aided-design (cad) model-assisted absolute three--dimensional shape measurement. Appl Opt 2017;56(24):6770–6.
[125] An Y, Zhang S. Pixel-by-pixel absolute phase retrieval assisted by an additional three-dimensional scanner. Appl Opt 2019;58(8):2033–41.
[126] Hyun J-S, Zhang S. Enhanced two-frequency phase-shifting method. Appl Opt 2016;55(16):4395–401.
[127] Yun H, Li B, Zhang S. Pixel by pixel absolute three-dimensional shape measurement with modified fourier transform profilometry. Appl Opt 2017;56(5):1472–80.
[128] Yang X, Zeng C, Luo J, Lei Y, Tao B, Chen X. Absolute phase retrieval using one coded pattern and geometric constraints of fringe projection system. Appl Sci 2018;8(12).
[129] Lohry W, Zhang S. High-speed absolute three-dimensional shape measurement using three binary dithered patterns. Opt Express 2014;22(22):26752–62.
[130] Karpinsky N, Zhang S. Composite phase-shifting algorithm for three-dimensional shape compression. Opt Eng 2010;49(6):063604.
[131] Zhang S, Huang PS. Novel method for structured light system calibration. Opt Eng 2006;45(8):083601.
[132] Vo M, Wang Z, Hoang T, Nguyen D. Flexible calibration technique for fringe-projection-based three-dimensional imaging. Opt Lett 2010;35(19):3192–4.
[133] Zhou W-S, Su X-Y. A direct mapping algorithm for phase-measuring profilometry. J Mod Opt 1994.
[134] Wen Y, Li S, Cheng H, Su X, Zhang Q. Universal calculation formula and calibration method in fourier transform profilometry. Appl Opt 2010;49(34):6563–9.
[135] Xiao Y, Cao Y, Wu Y. Improved algorithm for phase-to-height mapping in phase measuring profilometry. Appl Opt 2012;51(8):1149–55.
[136] Guo H, He H, Yu Y, Chen M. Least-squares calibration method for fringe projection profilometry. Opt Eng 2005.
[137] Wen Y, Li S, Cheng H, Su X, Zhang Q. Universal calculation formula and calibration method in fourier transform profilometry. Appl Opt 2010.
[138] Zhao W, Su X, Chen W. Whole-field high precision point to point calibration method. Opt Lasers Eng 2018;111:71–9.
[139] Su X, Song W, Cao Y, Xiang L. Phase-height mapping and coordinate calibration simultaneously in phase-measuring profilometry. Opt Eng 2004;43(3):708–12.
[140] Cui S, Zhu X. A generalized reference-plane-based calibration method in optical triangular profilometry. Opt Express 2009;17(23):20735–46.
[141] Asundi A, Wensen Z. Unified calibration technique and its applications in optical triangular profilometry. Appl Opt 1999;38(16):3556–61.
[142] Huang J, Wu Q. A new reconstruction method based on fringe projection of three--dimensional measuring system. Opt Lasers Eng 2014;52(1):115–22.
[143] Li Y, Su X, Wu Q. Accurate phase-height mapping algorithm for pmp. J Mod Opt 2006;53(14):1955–64.
[144] Fujigaki M, Sakaguchi T, Murata Y. Development of a compact 3D shape measurement unit using the light-source-stepping method. Opt Lasers Eng 2016;85:9–17.
[145] Zhao W, Su X, Chen W. Discussion on accurate phase-height mapping in fringe projection profilometry. Opt Eng 2017;56(10). 1–11–11
[146] Luo H, Xu J, Binh NH, Liu S, Zhang C, Chen K. A simple calibration procedure for structured light system. Opt Lasers Eng 2014;57:6–12.
[147] Xu J, Douet J, Zhao J, Song L, Chen K. A simple calibration method for structured light-based 3D profile measurement. Opt Laser Technol 2013;48:187–93.
[148] Zhang Z. A flexible new technique for camera calibration. IEEE Trans Pattern Anal Mach Intell 2000;22(11):1330–4.
[149] Duane CB. Close-range camera calibration. Photogrammetric Eng 1971;37(8):855–66.
[150] Sobel I. On calibrating computer controlled cameras for perceiving 3-d scenes. Artif Intell 1974;5(2):185–98.
[151] Tsai R. A versatile camera calibration technique for high-accuracy 3D machine vision metrology using off-the-shelf tv cameras and lenses. IEEE J Robotics Automat 1987;3(4):323–44.
[152] Hu Q, Huang PS, Fu Q, Chiang F-P. Calibration of a three-dimensional shape measurement system. Opt Eng 2003;42(2):487–93.
[153] Mao X, Chen W, Su X. Improved fourier-transform profilometry. Appl Opt 2007;46(5):664–8.
[154] Zappa E, et al. Fourier-transform profilometry calibration based on an exhaustive geometric model of the system. Opt Laser Eng 2009;47(7):754–67.
[155] Guo H, Chen M, Zheng P. Least-squares fitting of carrier phase distribution by using a rational function in fringe projection profilometry. Opt Lett 2006;31(24):3588–90.
[156] Du H, Wang Z. Three-dimensional shape measurement with an arbitrarily arranged fringe projection profilometry system. Opt Lett 2007;32(16):2438–40.
[157] Huang L, Chua PS, Asundi A. Least-squares calibration method for fringe projection profilometry considering camera lens distortion. Appl Opt 2010;49(9):1539–1548.
[158] Vo M, Wang Z, Pan B, Pan T. Hyper-accurate flexible calibration technique for fringe-projection-based three-dimensional imaging. Opt Express 2012;20(15):16926–41.
[159] Li Z, Shi Y, Wang C, Wang Y. Accurate calibration method for a structured light system. Opt Eng 2008;47(5):1–9.
[160] Audet S, Okutomi M. A user-friendly method to geometrically calibrate projector–camera systems. In: 2009 IEEE computer society conference on computer vision and pattern recognition workshops; 2009. p. 47–54.
[161] Yin Y, Peng X, Li A, Liu X, Gao BZ. Calibration of fringe projection profilometry with bundle adjustment strategy. Opt Lett 2012;37(4):542–4.
[162] Gao W, Wang L, Hu Z. Flexible method for structured light system calibration. Opt Eng 2009;47(8):1–10.

[163] Villa J, Araiza M, Alaniz D, Ivanov R, Ortiz M. Transformation of phase to (x,y,z)-coordinates for the calibration of a fringe projection profilometer. Opt Lasers Eng 2012;50(2):256–61.
[164] Li B, Zhang S. Structured light system calibration method with optimal fringe angle. Appl Opt 2014;53(33):7942–50.
[165] Huang Z, Xi J, Yu Y, Guo Q. Accurate projector calibration based on a new point–to-point mapping relationship between the camera and projector images. Appl Opt 2015;54(3):347–56.
[166] Chen R, Xu J, Chen H, Su J, Zhang Z, Chen K. Accurate calibration method for camera and projector in fringe patterns measurement system. Appl Opt 2016;55(16):4293–300.
[167] Suresh V, Holton J, Li B. Structured light system calibration with unidirectional fringe patterns. Opt Lasers Eng 2018;106:86–93.
[168] Wong E, Heist S, Bräuer-Burchardt C, Babovsky H, Kowarschik R. Calibration of an array projector used for high-speed three-dimensional shape measurements using a single camera. Appl Opt 2018;57(26):7570–8.
[169] Li B, Karpinsky N, Zhang S. Novel calibration method for structured light system with an out-of-focus projector. Appl Opt 2014;53(13):3415–26.
[170] Bell T, Zhang S. Method for out-of-focus camera calibration. Appl Opt 2016;55(9):2346–52.
[171] Holton JJ, Li B. Calibration method for spinning fringe projection: proof-of-concept. Opt Eng 2019;57(1):1–7.
[172] Zhu F, Liu W, Shi H, He X. Accurate 3D measurement system and calibration for speckle projection method. Opt Lasers Eng 2010;48(11):1132–9.
[173] Li D, Liu C, Tian J. Telecentric 3D profilometry based on phase-shifting fringe projection. Opt Express 2014;22(26):31826–35.
[174] Li B, Zhang S. Flexible calibration method for microscopic structured light system using telecentric lens. Opt Express 2015;23(20):25795–803.
[175] Liu H, Lin H, Yao L. Calibration method for projector-camera-based telecentric fringe projection profilometry system. Opt Express 2017;25(25):31492–508.
[176] Hu Y, Chen Q, Feng S, Tao T, Asundi A, Zuo C. A new microscopic telecentric stereo vision system - calibration, rectification, and three-dimensional reconstruction. Opt Lasers Eng 2019;113:14–22.
[177] Rao L, Da F, Kong W, Huang H. Flexible calibration method for telecentric fringe projection profilometry systems. Opt Express 2016;24(2):1222–37.
[178] Liu X, Cai Z, Yin Y, Jiang H, He D, He W, et al. Calibration of fringe projection profilometry using an inaccurate 2d reference target. Opt Lasers Eng 2017;89:131–7.
[179] Xiao Y-L, Xue J, Su X. Robust self-calibration three-dimensional shape measurement in fringe-projection photogrammetry. Opt Lett 2013;38(5):694–6.
[180] Leandry I, Breque C, Valle V. Calibration of a structured-light projection system: development to large dimension objects. Opt Lasers Eng 2012;50(3):373–9.
[181] An Y, Bell T, Li B, Xu J, Zhang S. Novel method for large range structured light system calibration. Appl Opt 2016;55(33):9563–72.
[182] Wang P, Wang J, Xu J, Guan Y, Zhang G, Chen K. Calibration method for a large-scale structured light measurement system. Appl Opt 2017;56(14):3995–4002.
[183] Huang PS, Hu Q, Jin F, Chiang F-P. Color-encoded digital fringe projection technique for high-speed 3-d surface contouring. Opt Eng 1999;38(6):1065–1071–7.
[184] Gong C, Li B, Harding KG, Zhang S. Comparing digital-light-processing (dlp) and liquid-crystal-on-silicon (lcos) technologies for high-quality 3D shape measurement. In: Proc. SPIE; vol. 9276 of SPIE sensing technology + applications. Baltimore, Maryland; 2014. p. 92760Q.
[185] Zhang Q, Su X, Cao Y, Li Y, Xiang L, Chen W. Optical 3-d shape and deformation measurement of rotating blades using stroboscopic structured illumination. Opt Eng 2005;44(11):1–7.
[186] Pan J, Huang PS, Chiang F-P. Color phase-shifting technique for three-dimensional shape measurement. Opt Eng 2006;45(2):013602.
[187] Hornbeck LJ. Digital light processing for high-brightness high-resolution applications. Proc SPIE 1997;3013:27–40.
[188] Zhang S, Huang PS. High-resolution real-time three-dimensional shape measurement. Opt Eng 2006;45(12):123601.
[189] Zhang S, van der Weide D, Oliver J. Superfast phase-shifting method for 3-d shape measurement. Opt Express 2010;18(9):9684–9.
[190] Gong Y, Zhang S. Ultrafast 3-d shape measurement with an off-the-shelf dlp projector. Opt Express 2010;18(19):19743–54.
[191] Li B, Zhang S. Novel method for measuring dense 3D strain map of robotic flapping wings. Meas Sci Technol 2018;29(4):45402.
[192] Zuo C, Tao T, Feng S, Huang L, Asundi A, Chen Q. Micro fourier transform profilometry ($\mu$ftp): 3D shape measurement at 10,000 frames per second. Opt Lasers Eng 2018;102:70–91.
[193] Chen Z, Wang X, Liang R. Snapshot phase shift fringe projection 3D surface measurement. Opt Express 2015;23(2):667–73.
[194] Li B, Ou P, Zhang S. High-speed 3D shape measurement with fiber interference. In: Proc. SPIE; vol. volume 9203 of series SPIE optics and photonics. San Diego, California; 2014. p. 920310. (invited)
[195] Gao W, Kemao Q. Parallel computing in experimental mechanics and optical measurement: a review. Opt Lasers Eng 2012;50(4):608–17.
[196] Wang T, Kemao Q. Parallel computing in experimental mechanics and optical measurement: a review (ii). Opt Lasers Eng 2018;104:181–91.
[197] Zhang S, Royer D, Yau S-T. Gpu-assisted high-resolution, real-time 3-d shape measurement. Opt Express 2006;14(20):9120–9.
[198] Liu K, Wang Y, Lau DL, Hao Q, Hassebrook LG. Dual-frequency pattern scheme for high-speed 3-d shape measurement. Opt Express 2010;18(5):5229–44.
[199] Feng S, Chen Q, Zuo C. Graphics processing unit-assisted real-time three--dimensional measurement using speckle-embedded fringe. Appl Opt 2015;54(22):6865–73.
[200] Wang H, Zeng H, Chen P, Liang R, Jiang L. Fast single fringe-pattern processing with graphics processing unit. Appl Opt 2019;58(25):6854–64.
[201] Wang J, Xiong Z, Wang Z, Zhang Y, Wu F. Fpga design and implementation of kinect-like depth sensing. IEEE Trans Circuits Syst Video Technol 2016;26(6):1175–86.
[202] Zhan G, Tang H, Zhong K, Li Z, Shi Y, Wang C. High-speed fpga-based phase measuring profilometry architecture. Opt Express 2017;25(9):10553–64.
[203] Chen B, Zhang S. High-quality 3D shape measurement using saturated fringe patterns. Opt Laser Eng 2016;87:83–9.
[204] Zhang S, Yau S-T. High dynamic range scanning technique. Opt Eng 2009;48(3):033604.
[205] Waddington C, Kofman J. Analysis of measurement sensitivity to illuminance and fringe-pattern gray levels for fringe-pattern projection adaptive to ambient lighting. Opt Laser Eng 2010;48:251–6.
[206] Jiang C, Bell T, Zhang S. High dynamic range real-time 3D shape measurement. Opt Express 2016;24(7):7337–46.
[207] Zheng Y, Wang Y, Suresh V, Li B. Real-time high-dynamic-range fringe acquisition for 3D shape measurement with a rgb camera. Meas Sci Technol 2019;30:075202.
[208] Suresh V, Wang Y, Li B. High-dynamic-range 3D shape measurement utilizing the transitioning state of digital micromirror device. Opt Laser Eng 2018;107:176–181.
[209] Salahieh B, Chen Z, Rodriguez JJ, Liang R. Multi-polarization fringe projection imaging for high dynamic range objects. Opt Express 2014;22:10064–71.
[210] Qi Z, Wang Z, Huang J, Xue Q, Gao J. Improving the quality of stripes in structured-light three-dimensional profile measurement. Opt Eng 2016;56(3):031208.
[211] Long Y, Wang S, Wu W, Liu K. Accurate identification of saturated pixels for high dynamic range measurement. Opt Eng 2015;54(4):043106.
[212] Zhong K, Li Z, Zhou X, Li Y, Shi Y, Wang C. Enhanced phase measurement profilometry for industrial 3D inspection automation. Int J Adv Manuf Technol 2015;76(9):1563–74.
[213] Rao L, Da F. High dynamic range 3D shape determination based on automatic exposure selection. J Vis Commun Image Represent 2018;50:217–26.
[214] Song Z, Jiang H, Lin H, Tang S. A high dynamic range structured light means for the 3D measurement of specular surface. Opt Laser Eng 2017;95:8–16.
[215] Feng S, Chen Q, Zuo C, Asundi A. Fast three-dimensional measurements for dynamic scenes with shiny surfaces. Opt Comm 2017;382:18–27.
[216] Wang Y, Zhang J, Luo B. High dynamic range 3D measurement based on spectral modulation and hyperspectral imaging. Opt Express 2018;26(26):34442–50.
[217] Lin H, Gao J, Mei Q, He Y, Liu J, Wang X. Three-dimensional shape measurement technique for shiny surfaces by adaptive pixel-wise projection intensity adjustment. Opt Lasers Eng 2017;91:206–15.
[218] Lin H, Gao J, Mei Q, He Y, Liu J, Wang X. Adaptive digital fringe projection technique for high dynamic range three-dimensional shape measurement. Opt Express 2016;24:7703–18.
[219] Li D, Kofman J. Adaptive fringe-pattern projection for image saturation avoidance in 3D surface-shape measurement. Opt Express 2014;22:9887–901.
[220] Jiang H, Zhao H, Li X. High dynamic range fringe acquisition: a novel 3-d scanning technique for high-reflective surfaces. Opt Laser Eng 2012;50:1484–93.
[221] Zhao H, Liang X, Diao X, Jiang H. Rapid in-situ 3D measurement of shiny object based on fast and high dynamic range digital fringe projector. Opt Laser Eng 2014;54:170–4.
[222] Ekstrand L, Zhang S. Auto-exposure for three-dimensional shape measurement with a digital-light-processing projector. Opt Eng 2011;50(12):123603.
[223] Chen C, Gao N, Wang X, Zhang Z. Adaptive projection intensity adjustment for avoiding saturation in three-dimensional shape measurement. Meas Sci Technol 2018;410:694–702.
[224] Feng S, Zhang Y, Chen Q, Zuo C, Li R, Shen G. General solution for high dynamic range three-dimensional shape measurement using the fringe projection technique. Opt Laser Eng 2014;59:56–71.
[225] Ri S, Fujigaki M, Morimoto Y. Intensity range extension method for three-dimensional shape measurement in phase- measuring profilometry using a digital micromirror device camera. Appl Opt 2008;47:5400–7.
[226] Zhang L, Chen Q, Zuo C, Feng S. High dynamic range 3D shape measurement based on the intensity response function of a camera. Appl Opt 2018;57(6):1378–86.
[227] Babaie G, Abolbashari M, Farahi F. Dynamics range enhancement in digital fringe projection technique. Precis Eng 2015;39:243–51.
[228] Sheng H, Xu J, Zhang S. Dynamic projection theory for fringe projection profilometry. Appl Opt 2017;56(30):8452–9460.
[229] Feng S, Zhang L, Zuo C, Tao T, Gu G. High dynamic range 3D measurements with fringe projection profilometry: a review. Meas Sci Technol 2018;29:122001.
[230] Qi Z, Wang Z, Huang J, Xing C, Gao J. Highlight removal based on the regional-projection fringe projection method. Opt Eng 2018;57(4):041404.
[231] Cai Z, Liu X, Peng X, Yin Y, Li A, Wu J, et al. Structured light field 3d imaging. Opt Express 2016;24(18):20324–34.
[232] Liu G-h, Liu X-Y, Feng Q-Y. 3D shape measurement of objects with high dynamic range of surface reflectivity. Appl Opt 2011;50(23):4557–65.
[233] Laughner JI, Zhang S, Li H, Shao CC, Efimov IR. Mapping cardiac surface mechanics with structured light imaging. Am J Physiol - Heart Circulatory Physiol 2002;303(6):H712–20.
[234] Zhe Zhang HGPH, Nejat G. A novel 3D sensory system for robot-assisted mapping of cluttered urban search and rescue environments. Intell Serv Robot 2011;4(2):4–10.
[235] Xu J, Wang P, Yao Y, Liu S, Zhang G. 3D multi-directional sensor with pyramid mirror and structured light. Opt Lasers Eng 2017;93:156–63.
[236] Rao G, Wang G, Yang X, Xu J, Chen K. Normal direction measurement and optimization with a dense three-dimensional point cloud in robotic drilling. IEEE/ASME Trans Mechatron 2017;23(3):986–96.

[237] Xu J, Rao G, Chen Z. Robotic visual servoing using fringe projection profilometry. In: Optical Metrology and Inspection for Industrial Applications V, 10819. International Society for Optics and Photonics; 2018. p. 108190Q.
[238] Li H, Adams B, Guibas LJ, Pauly M. Robust single-view geometry and motion reconstruction. ACM Trans Graph 2009;28(5):175:1–175:10.
[239] Li H, Sumner R, Pauly M. Global correspondence optimization for non-rigid registration of depth scans. Comput Graphics Forum 2008;27:1421–30.
[240] Wang P, Xu J, Guan Y, Zhang G, Chen K. Three-dimensional panoramic sensor based on a variable-frequency fringe pattern. Appl Opt 2017;56(3):620–5.
[241] Chen R, Wang G, Zhao J, Xu J, Chen K. Fringe pattern based plane-to-plane visual servoing for robotic spray path planning. IEEE/ASME Trans Mechatron 2018;23(3):1083–91.
[242] Li J, Chen Z, Rao G, Xu J. Structured light-based visual servoing for robotic pipe welding pose optimization. IEEE Access 2019. doi:10.1109/ACCESS.2019.2943248.
[243] NIJ. Forensic science technology working group operational requirements. https://www.nij.gov/topics/forensics/documents/2018-11-forensic-twg-table.pdf; 2018.
[244] NIST. Testing & validation of 3D imaging technologies for footwear & tire impressions evidence. https://www.nist.gov/sites/default/files/documents/forensics/osac/SAC-Phy-Footwear-Tire-Sub-R-D-004-3D-Scanning_Revisions_Mar_2016.pdf; 2016.
[245] Radiohead. The making-of ”house of cards” video. https://www.youtube.com/watch?v=cyQoTGdQywY; 2008a.
[246] Radiohead. Radiohead - house of cards. https://www.youtube.com/watch?v=8nTFjVm9sTQ; 2008b.
[247] Macklin M.. Opengl radiohead house of cards visualizer. https://www.youtube.com/watch?v=03_nelTJlVo; 2008.
[248] PartiallyFrozen. Radiohead - solarstone - house of cards. https://www.youtube.com/watch?v=cd5AiQddF2U; 2008.
[249] Yao B, Imani F, Sakpal AS, Reutzel EW, Yang H. Multifractal analysis of image profiles for the characterization and detection of defects in additive manufacturing. J Manuf Sci Eng 2018;140(3):31014.
[250] Stavroulakis P, Leach RK. Invited review article: review of post-process optical form metrology for industrial-grade metal additive manufactured parts. Rev Sci Instrum 2016;87(4):41101.
[251] Land II WS, Zhang B, Ziegert J, Davies A. In-situ metrology system for laser powder bed fusion additive process. Procedia Manuf 2015;1:393–403.
[252] Kalms M, Narita R, Thomy C, Vollertsen F, Bergmann RB. New approach to evaluate 3D laser printed parts in powder bed fusion-based additive manufacturing in-line within closed space. Addit Manuf 2019;26:161–5.
[253] Zhang B, Ziegert J, Farahi F, Davies A. In situ surface topography of laser powder bed fusion using fringe projection. Addit Manuf 2016;12:100–7.
[254] Li Z, Liu X, Wen S, He P, Zhong K, Wei Q, et al. In situ 3D monitoring of geometric signatures in the powder-bed-fusion additive manufacturing process via vision sensing methods. Sensors 2018;18(4):1180.
[255] Garmendia I, Leunda J, Pujana J, Lamikiz A. In-process height control during laser metal deposition based on structured light 3D scanning. Procedia Cirp 2018;68:375–80.